Imaging Early Oceanic Crust Spreading in the Equatorial Atlantic Ocean: Insights from the MAGIC Wide-angle Experiment

Maryline Moulin, Philippe Schnurle, Alexandra Afilhado, Flora Gallais, Nuno Dias, Mikael Evain, José Soares, Reinhardt Fuck, Otaviano da Cruz, Pessoa Neto, et al.

Imaging Early Oceanic Crust Spreading in the Equatorial Atlantic Ocean: Insights from the MAGIC Wide-angle Experiment

Maryline Moulin(1), Philippe Schnurle(1), Alexandra Afilhado(2,3), Flora Gallais(1), Nuno Dias(2,3), Mikael Evain(1), José Soares(4), Reinhardt Fuck(4), Otaviano da Cruz Pessoa Neto(5), Adriano Viana(5), Daniel Aslanian(1) & MAGIC Team(1,2,3,4,5,6,7,8)

(1) Ifremer, Department of Marine Geosciences, BP 70, 29280 Plouzané, France
(2) ISEL - Instituto Superior de Engenharia de Lisboa, Lisboa, Portugal
(3) IDL – Instituto Dom Luis, Lisboa, Faculdade das Ciências da Universidade de Lisboa, 1749-016 Lisboa, Portugal.
(4) Instituto de Geociências – Lablithos, Universidade de Brasilia, Campus Darcy Ribeiro, 70910-900 Brasilia, Brazil.
(5) Petrobras S.A., Research Center, CENPES, PROFEX, Rio de Janeiro, Brazil
(6) LETG-Nantes Geolittomer, Université de Nantes, Campus Tertre, BP 81227, 44312 Nantes Cedex 3, France
(7) IUEM, Domaines Océaniques, CNRS, 29280 Plouzané, France
(8) Departemento de Geofisica, Universidade Federal de Pampa, Campus Caçapava do Sul, 96570000 Caçapava do Sul, RS, Brazil

Abstract

During the MAGIC (Margins of brAzil, Ghana, and Ivory Coast) experiment, five combined wide-angle, and reflection seismic profiles were acquired in the Pará-Maranhão/Barreirinhas/Ceará basins northern Brazil. This is a pull-apart passive margin, with two strike-slip borders. The equipment deployed includes 143 sea-bottom seismometers (OBS), a 4.5-km seismic streamer, and a 7587-in^3 airgun array. In this paper, we focus on the distal parts of three profiles, and one entire transverse NW-SE profile, located on the presumed Cretaceous oceanic crust.

Forward modelling of these wide-angle data sets reveals an E-W lateral evolution of the oceanic crust spreading initiation with: 1) just after the so-called intermediate

domain, 60 km-wide domain that consists of a 5-km-thick crystalline crust. The basement presents two layers characterized by high acoustic velocity. This domain is bounded to the NW by a NW-SE volcanic line (Volcano Alignment), and 2) a 5-km-thick oceanic crust consisting of two layers characterized by “normal velocities” spanning between the two main fracture zones that fringe the Pará-Maranhão-Barreirinhas-Ceará segment. Despite a similar thickness, these two sub-domains present different velocity distribution in their two layers. They are both overlain by 5.5 km of sedimentary deposits. Forward wide-angle modelling confirms that the seafloor spreading process was progressive, with firstly the emplacement of a proto-oceanic crust, and then a thin oceanic crust. The “proto-oceanic” crust presents a similar seismic velocity with the intermediate domain interpreted as exhumed lower continental crust except for the lower part where the intruded lower crust gives place to a very sharp Moho at the base of the proto-oceanic domain. By contrast, the thin oceanic crust domain has a lower velocity structure in its upper layer, that is interpreted as basalt and is absent in the proto-oceanic crust. This eastward evolution, as also observed in the Provençal Basin, and the Santos Basin, suggests the involvement of the lower continental crust in the first steps of seafloor spreading.

Keywords

Equatorial Atlantic Ocean, Brazil, Pará-Maranhão-Barreirinhas-Ceará basins, wide-angle seismic, oceanic crust, intermediate domain.

1 Introduction

The equatorial Brazilian margin, which is the focus of the MAGIC (Margins of brAzil, Ghana, and Ivory Coast) research experiment, represents a unique natural laboratory for addressing fundamental questions on strike-slip margins. The MAGIC experiment is a joint project of the Department of Marine Geosciences (IFREMER: Institut Français de Recherche pour l’Exploitation de la MER, France), the Laboratory of « Oceanic Geosciences » (IUEM: Institut Universitaire et Européen de la Mer, France), the Faculdade de Ciências da Universidade de Lisboa (IDL, Portugal), the Universidade de Brasilia (Brazil), and PETROBRAS (Brazil). The main goals of the MAGIC experiment are (i) to investigate the deep structure of the Pará-Maranhão-Barreirinhas-Ceará basins, N-NE Brazil, (ii) to characterize the segmentation and the nature of the crust in the different domains of this passive margin, between the unthinned continental crust and the true oceanic crust, and (iii) to understand the fundamental processes that lead to the thinning, and finally to the breakup of the continental crust in the specific context of a pull-apart system with two strike-slip borders. This paper presents the results of P-wave velocity modelling on coincident near-vertical reflection multi-channel seismic (MCS) and, wide-angle seismic data sets in an area that is supposed to be of oceanic nature.

2 Geological setting and previous work

The Pará-Maranhão-Barreirinhas-Ceará margin (Figure 1) is located in the southward second 600-800-km-wide segment of the Equatorial Atlantic Ocean, between the São Paulo Fracture Zone to the north, and the Chain Fracture Zone to the south. The Equatorial Atlantic Ocean can itself be interpreted as a "transfer zone" between two main oceans resulting from two ruptures during two global geodynamic revolutions (Moulin & Aslanian, 2010; Leroux *et al.,* 2018): the opening of the Central Atlantic Ocean that started by Sinemurian time (Sahabi *et al.,* 2004), and the opening of the South Atlantic Ocean in Hauterivian time (Rabinowitz & LaBrecque 1979; Austin & Uchupi 1982; Curie 1984; Moulin *et al.* 2010a), which started about 60 My later and shifted about 30° to the east respect to the Central Atlantic.

Despite the lack of magnetic lineaments due to its position close to the equator, the beginning of seafloor spreading on this portion of the ocean is dated to Cretaceous time, separating Africa from South America. Besides the exact date still being debated between Aptian (112 Ma) (Blarez, 1986; Mascle and Blarez, 1987; Gouyet, 1988; Azevedo, 1991; Matos, 1992), and Upper Albian (100 Ma) (Oliveira Marinho, 1985; Gouyet, 1988; Basile et al., 2005; Torsvik et al., 2009; Heine et al., 2013; Granot & Dyment, 2015), the major unknown on this segment is the formation and evolution of the conjugate system (Pará-Maranhão-Barreirinhas-Ceará and the Deep Ivory Basin-Ghana Platform). This fact is primarily because, until the MAGIC experiment, all data were collected on the African margin (Mascle et al., 1988; Basile et al., 1993; Mascle et al., 1995; Sage, 1994; Pierce et al., 1996; Edwards et al., 1997; Sage et al., 1997; Antobreh *et al.*, 2009). Studies based on seismic refraction data published in the 1990s only concern the southern strike-slip boundary of the African system, and not the entire Pará-Maranhão-Barreirinhas-Ceará/Ghana-Ivory coast pull-apart system.

These previous results based on refraction and IODP (Integrated Oceanic Drilling

Program data provided an image of the deep structure of the southern limit of the African side of this pull-apart system, where continental crust thickness never exceeds 20 km (Figure 2). This layered continental crust thins abruptly southwards, across the Ghana-Ivory Coast (GIC) Ridge, reaching directly the younger oceanic crust from the next segment, south of the Romanche Fracture Zone. In the divergent part of the pull-apart system, the initial position of the South American plate respect to the African one, before any horizontal movement, the position and the age of the oldest oceanic crust are still a matter of debate (Torsvik et al., 2009; Moulin et al., 2010; Aslanian and Moulin, 2010; Heine et al., 2013; Muller et al., 2016). Whilst the Landward Limit Oceanic Crust (LaLOC) defined by Heine et al. (2013) is supposed to represent the first inset of oceanic crust, neither of the two flow-lines parallel wide-angle profiles from the EQUAREF experiment shows clear evidence of oceanic crust (Figure 2). Whilst on the EQUAREF-1 profile, Pierce *et al. (*1996) concluded that the extreme western end of the profile exhibits a 10-11-km-thick crust with a velocity typical of thinned continental crust (3.2 to 3.6 km/s and 6.8 km/s), Sage (1994) proposed the presence of oceanic crust only westwards of IODP site 961, at the westernmost end of the profile, between their OBS-3 and OBS-4 on the EQUAREF-7 profile. This position is 50 to 100 km westwards of the LaLOC (Figure 2).

On the Brazilian side, no refraction data were available before the MAGIC experiment, but this margin benefits from a good coverage of industrial ultra-deep high-quality seismic lines. The interpretation of these industrial profiles suggests a huge discrepancy in the position of the presumed oceanic crust (Figure 1b), and the LaLOC of Heine *et al.* (2013). Aslanian et al., 2021, who presented two another MAGIC P-wave velocities modelling, reveal distinct structural domains from onshore Brazil towards the Atlantic Ocean characterized by variations of the crustal thicknesses and velocities: (1) an unthinned continental crust below the São Luís Craton, where the crust is 33 km thick, (2) a 60 km wide necking domain; (3) offshore, east of the continental slope, a 10km-thick deep sedimentary basin (basin I and II); (4) eastwards, the limit of the previous domain is marked by NW-SE aligned volcanoes and the inception of the oceanic domain.

3. Data acquisition, quality and processing

During the MAGIC experiment, five coincident Multi-Channel Seismic (MCS) reflection and wide-angle seismic profiles, sub-bottom high-resolution (CHIRP) profiles, calypso cores, and bathymetry data were collected on the Pará-Maranhão-Barreirinhas-Ceará basins (Figure 1). The seismic reflection data were acquired using a 4.5 km, 360-channel digital streamer, and a tuned airgun array of 7587 in^3, towed at a depth of 18-–25 m. A total of 143 ocean bottom seismometer/hydrophones (OBS/OBH) from Ifremer (Auffret *et al.*, 2004), and the University of Brest were deployed, spaced every 7 nautical miles (~13 km). Three seismic profiles, perpendicular to the margin, were extended onshore by land seismic stations (LSS) (Figure 1) (see Aslanian *et al.*, 2021). The seismic source consisted of a tuned array of 18 airguns ranging from 250 in^3 G-guns to 9 L Bolt airguns, with main frequencies centred around 10-15 Hz. Shots occurred at a constant time interval of 60 s (firing rate), resulting in intervals of about 150 m between shots. A total of 12382 shots (profile MC-1: 3032, MC-2: 1741, MC-3: 2834, MC-4: 1145, and MC-5: 3801) were fired by the air gun array, recorded simultaneously on MCS reflection and wide-angle seismic profiles.

This paper focuses on profile MC1 and the distal parts of crossing profiles MC2, MC3 and MC4. The MC1 profile (Figure 1) is about 360 km long and is located entirely on the presumed oceanic-floored basin, except on its south-easternmost part. It spans the entire domain between the two main fracture zones that fringe the Pará-Maranhão-Barreirinhas-Ceará segment: the São Paulo Double Fracture Zone (FZ) to the north and the Romanche FZ to the south. Twenty-five OBS were deployed along this profile (Figure 1). Shots were acquired from MC1OBS25 until MC1OBS02 where the water depth shallows to less than 100 m. MC1OBS01 is hence not corrected from its deployment position, since the water arrival does not provide sufficient constraints to be able to relocate it.

Pre-processing of the OBS data included calculation of the clock-drift corrections to adjust the clock in each instrument to the GPS base time. Instrument locations were corrected for drift from the deployment position during their descent to the seafloor using the direct wave water arrival. The drift of all instruments did not exceed 200 m. All the instruments were recovered and provided useful data on all four channels. Data quality along the profile was generally highly satisfactory with clear arrivals to offsets over 100 km between the ship and the seafloor instrument. Picking of the onset of first and secondary arrivals was performed without filtering where possible (mostly between offsets of 0 and 40 km). Further processing of the data to facilitate picking at larger offsets included deconvolution, application of a bandpass-filtering (1-6-48-64 Hz), and trace normalization.

All the seafloor instruments provide equally good quality of data and seismic record sections in the presumed oceanic basin are remarkably similar, suggesting that the crustal structure has a minor lateral variation (Figure 3). OBS 9, 11, 18 and 24 were selected to show the quality of the data used to constrain the forward modelling (Figures 4 to 7). Useful arrivals could be picked up to a 40-160 km offset, including arrivals reflected from the Moho (PmP) and refracted in the shallow mantle (Pn) (Figure 4).

Processing of the multichannel seismic data was performed using the Geovecteur processing package. The processing sequence of the reflection seismic data was composed of geometry (including streamer feathering), CMP binning at 12.5 m intervals and sorting, bandpass filter (2–16–64–96 Hz), re-sampling from 2 to 4 ms. After velocity analysis, true amplitude recovery was applied plus normal move-out, multiple attenuation, time-variant bandpass filter (from 2–16–48–64 at sea bottom to 2–16–32–48 Hz 3 s below), inside and outside mute, stack and post-stack time-variant bandpass filter and Kirchhoff time migration.

4. Forward Modelling

The data were modelled by using an iterative procedure of two-dimensional forward ray-tracing followed by a damped least-squares travel-time inversion with the RAYINVR software (Zelt & Smith, 1992). The wide-angle modelling proceeds in a top-to-down strategy of arrival time fitting of the reflected and refracted phases identified in the sedimentary section. For each sedimentary sequence, we correlated the two-way travel times of its base, from the MCS section, with the arrival times of the reflected and refracted phases identified in the OBS data.

An iterative procedure of velocity and depth adjustment, with control of the depth-twtt (two way travel-time) conversion against MCS data, was then applied. This procedure was applied to all sedimentary layers down to the basement. For the basement, we only used arrival times from the OBS and LSS data set. The iterative procedure stops when an appropriate fit of the arrival times from both OBS and MCS data is reached, i.e., the stopping criteria is a normalized chi-square of 1.

To constrain velocity gradients and velocity contrasts at the interfaces of the model, we performed amplitude modelling (Zelt & Ellis, 1988), which is a trial and error procedure. Amplitude modelling is based on the variation of the angle of incidence of the transmitted and reflected seismic energy across boundaries; therefore, synthetic record sections should reproduce the observed offset variations of amplitude. Furthermore, for each incidence angle, the fractions of transmitted and reflected P-wave energy (relative to the total incident energy) depend on the impedance contrast across interfaces; thus, synthetic record sections should reproduce the relative amplitudes amongst all the arrivals. Another important constraint provided by the amplitude modelling is the thickness and velocity gradient in each layer.

The final velocity model of the MC1 profile images the sedimentary and crustal layers to a depth of around 20 km (Figure 8). The model is composed of five sedimentary layers (S1 to S5), 5.5 km thick in total, with top and bottom seismic velocities of 1.8 and 2.2 km/s (S1), 2.4 and 2.75 km/s (S2), 2.9 and 3.0 km/s (S3), 3.75 km/s (S4), and 4.15 and 4.2 km/s (S5). Near the intersection with the Romanche FZ (at a distance of 280 km form the model), the velocity increases in layer S4 (4.5 to 4.75 km/s) and layer S5 (5.0 to 5.5 km/s). The velocity increases gradually inside the sedimentary column and no velocity inversion is identified in this profile, in contrast to what is observed, westwards, in the deep basin of the Pará-Maranhão/Barreirinhas/Ceará margin (Aslanian *et al,*. 2021). The model comprises a two-layered (upper and lower) crust above a lithospheric mantle layer (Figure 8). The upper crustal layer was set to less than 1.5 km thickness, with top-bottom velocities of 5.7-5.9 km/s (on the northwestern part), smoothly increasing from 5.9-6.0 km/s (on the southeastern part). The presence of this thin crust was added to the model to correctly predict time arrivals of the lower crust and to be coherent with MC3 P-wave velocities model. Lower crust velocities range from 6.2-6.8 km/s in the northwestern part of the profile to 6.2-7.2 km/s in the southeastern part. The thickness of the lower crust is ~4 km. All OBS seismic record sections show clear crustal refracted and reflected arrivals, from the lower crust (Pg2) and the crust-mantle boundary (Pm1P) (Figure 7). Finally, the lithospheric mantle velocity, constrained by Pn arrivals, varies from 8.2 to 8.7 km/s at 45 km depth. This high velocity in the upper mantle (8.7 km/s) is essential to be able to explain the high apparent velocity and strong amplitude of the Pn, visible up to 100-170 km offset on several OBS (Figures 4, 5 & 6).

5. Evaluation of the MC1 model

We have digitized a total of 35629 events and interpreted their respective phases. Travel-time uncertainty was estimated on the MC1OBS record and generally fixed at 0.100 s. The model fits the travel-time and phase of 34656 events, i.e. 97 % of all picks, with a global RMS travel-time residual of 0.060 s. Given the individual uncertainty of our events, the model results in a normalized chi-square of 0.356 (Table 1). Individually, the MC1 model explains the MC1OBSs with a chi-square lower or equal to 0.848 and RMS lower or equal to 0.095 s (Table 2). During the forward modelling, the most difficult element to constrain was the velocity of layers S3 and S4 due to the reduced number of picks (Table 1). Nevertheless, the RMS value for each phase varies from 0.017 s (Pw) to 0.097 s (Ps4), and the normalized chi-square varies from ~0.1 (short offset range of observation Ps2P), and ~0.875 (Ps4) (Table 1). Most interface nodes in the MC1 model produce a hit count larger than 200 rays (Figure 10b). The number of rays that constrain each velocity is always above 100 (Figure 10b). The resolution of the interface depth and velocity nodes is build from the diagonal terms of the inversion kernel, and is a measurement of the spatial averaging of the true earth structure by a linear combination of model parameters (Zelt, 1999). Typically, resolution matrix diagonals greater than 0.5–0.7 are said to indicate reasonably well-resolved model parameters (e.g. Lutter & Nowack 1990). The resolution is generally very good, above 0.9 (Figure 10d). The Spread-Point Function (SPF) suggests that smearing is low (Figure 10c). The SPF is build from the off-diagonal terms of the inversion kernel, and suggests that smearing is low (Figure 10c). In summary, the MC1 model is well constrained from arrival times, except for the velocity-gradient of the second crustal layer, which was set by amplitude modelling, considering the typical features of seismic wave propagation in a layered medium, namely the fit of cut-off and critical distances, as well as triplication of Pg2, Pm1P and Pn (Figure 4).

We have built a 2-D gravity model consisting of 170 homogeneous density blocks, by converting seismic velocity to density according to Ludwig *et al.* (1970). The density conversion of our velocity model can predict the main trend of the gravity anomaly, with a density of 3430-3460 kg/m^3 in the deep lithospheric mantle to remove the regional trend. The density ranges from 2200 to 2500 kg/m3 in the sedimentary basins, 2550 to 3000 kg/m3 in the igneous crust and 3430 kg/m3 to 3460 kg/m3 in the mantle (Figure 9a). Where the MC1 model is not covered by seismic rays, the largest differences among observed (red dotted lines in Figure 9b) and calculated gravity anomalies (black line in Figure 9) occur close to the continental slope with a maximum difference reaching 50 mGal. Generally, the observed and calculated gravity anomalies are similar (Figure 9b).

It worth to note that the thickness of the unthinned continental crust, set to ~21 km, on the southeastern end of the model, is based on gravity modelling only (Figure 9) and the information provided by the MC5 modelling.

6. Comparison to reflection seismic data

The MAGIC1 MCS profile starts in the middle of the continental slope with ~3 s twtt sedimentary layers (Figure 11). These sediment layers thicken to 3.5 s twtt into the distal part (Northwards). The four shallowest layers are well individualised and stratified, but the absence of well-imaged reflectors in the fifth one makes it difficult to define its top. Nevertheless, the top of the acoustic basement and reflections from the Moho are well-marked by a strong reflector at 8 s, and a discontinuous one at 9 s twtt, between 160 and 280 km model distance. This strong and discontinuous reflector disappears between 0 and 160 km model distance. It is important to note that the base of the first crustal layer does not correspond to a seismic reflector nor a change in the seismic facies, as noticed on the MAGIC3 profile (Aslanian et al., 2021) but needed by wide-angle modelling. In the northern part of the profile, crustal arrivals (top of basement and Moho) are interpreted from the seismic wide-angle data only.

To verify the accuracy of the wide-angle velocity model, we also performed a Pre-Stack Depth Migration (PSDM) of the MCS data by using the MC1 final P-wave velocity model (Figure 12). The pre-processing sequence is identical to the MCS data time processing and includes geometry, wave-equation multiple attenuation, shot-gather predictive deconvolution, time-variant bandpass filter, and random multiple attenuation. Hence, if the velocity model used for the depth migration is close to the true medium velocity, all common offset migrated panels map the recorded seismic events to the same reflector depth. If the velocity is under/over estimated, the residual move-out from near to far offset at selected common-mid points along the MCS profile can be estimated trough semblance analysis and translated into an interval velocity correction (Liu & Bleistein, 1995). This provides discussion as to the real geometry of the main features imaged by the MC1 profile. The PSDM of MC1 strongly improves the seismic imaging of the basement and sediments (especially in the centre of the profile and at its eastern extremity) (Figure 12). The PSDM MC1 profile shows a rather continuous seismic character with strong well-stratified and high-frequency reflectors and confirms the interpretation of the crustal structure (basement and Moho) (Figure 12).

Our interpretation of the ION-GXT lines (courtesy of Petrobras) provides additional information. In the oceanic domain, the ION-GXT 7000 line equivalent to MAGIC3 (Figure 1b) shows two sets of very strong deep reflectors in the typical oceanic domain at around 9 s twtt (around 12 km depth), 4 km below what appears to be the top of the basement, and the second set of deep reflectors at 11.5 s twtt, around a depth of 24 km below sea level, rising slowly oceanwards to 18 km at the end of the profile. Nevertheless, these deepest reflectors at 11.5 s twtt are seen neither on MCS MC1 profile nor on the crossing, perpendicular ION-GXT profiles, and their significance (out-of-plain, artefact, anisotropy or unidirectional reflectors?) and interpretation (intra oceanic, Moho or intra-mantellic reflectors?) need to be explored.

Deep reflectors in the oceanic crust are mostly interpreted as the manifestation of serpentinization along faults (Carton *et al.*, 2014) as the result of magma emplacement forming sills in the lower crust (Canales *et al.*, 2009) or frozen melt bodies representing relicts of a paleo melt channel system (Nedimovic *et al.*, 2005; Sauter *et al.*, 2016), a fossil melt-rich crust-mantle transition zone (Moho Transition Zone - MTZ) (Sauter *et al.*, 2016), or large shear zones that tapped a connection to deep lithospheric melt channels leading to magmatic intrusions within the crust and emplacement of post-seafloor-spreading volcanic edifices within deformation corridors (Sauter *et al.*, 2018). Wide-angle data are therefore crucial for the interpretation of deep crustal/mantellic reflectors on the MCS section. The modelled Moho, at 12.5 km depth, of the wide-angle seismic model of MC3 (Aslanian *et al.*, 2021) fits well with the first set of deep reflectors (Figure 13). At the base of the Mantle 1 layer, in the deep Basin I and II, the MC3 wide-angle seismic data recorded a very deep intra-mantle reflection (Pm2P) at a depth of 25 km. This reflection is associated with a very small step in the P-wave of 0.05 to 0.1 km/s. The flow line-oriented deep reflectors lying at <17 km, visible on the IONGXT7000 profile, may correspond to the prolongation of this intra-mantle reflector. P-wave velocities within this deepest Mantle 2 layer are 8.2-8.4 km/s from the continental domain to the oceanic domain.

7. 1D-VZ profiles and crustal nature

The interpretation of E-W wide-angle MAGIC MC3 profile has shown the presence of a deep basin interpreted as exhumed lower continental crust, with two different sub-basins I & II, followed by two different oceanic domains A & B (Figure 1; Aslanian *et al.*, 2021). The NW-SE MC1 profile is inside the Oceanic A domain, parallel to the external limit of the deep basin I highlighted in the north by a series of aligned volcanoes, and crosses the three MAGIC MC2, MC3 & MC4 profiles. To characterize the P-wave seismic velocity variations along this domain, 1-D velocity-depth (Vz) profiles were extracted from the velocity models at 10 km intervals (Figures 14 & 15). Figure 14 reveals a strong segmentation and abrupt passage at the two limits of the oceanic A domain (purple lines) respect to the intermediate domain (yellow and green lines) and to oceanic B domain (red lines). In oceanic A domain, the deepest crustal layer present in the deep Basin I (yellow lines in Figure 14) is absent whilst the Moho is characterized by a larger jump in velocity of about 1 km/s, at the same depth: the transition between the upper mantle and the crust is thus sharper. The 1D-Vz profiles of MC1 (Figure 15b) also homogeneously present a less than 1-km-thick upper crustal layer with a velocity of 5.8-6.0 km/s, which is not observed on the other profiles, except for MC4 (Figure 14a). Figure 15a presents the 1D-Vz profiles at the crossing points of MAGIC profiles. Despite an overall similarity in gradient and steep velocity variation, some discrepancies can be observed. While the MC1 profile, which samples a single homogeneous domain along the profile clearly shows a thin top layer at the top of the basement, this layer is not always identified on the MAGIC E-W profiles, probably due to the smaller sampled portion of this domain by these profiles. The increase in thickness of the upper crustal layer (2 km instead of 1 km) on the MC4 profile may thus explain its identification and may be related to the vicinity of the Volcano Alignment to the west (Figure 1).
The second steep change (Oceanic B – red profiles in Figure 14) is imaged by the MC3 and MC4 profiles, with a very strong lateral variation in the upper basement layer where velocity decreases towards the east to 4.8-5.1 km/s. On the one hand, the oceanic B domain has 1D-Vz profiles that match, even at a lower thickness, the shape, gradient and thickness ratio of the 1D-Vz profiles of 'normal' oceanic crust compiled

by White et al. (1992) and Christeson et al., 2019. In contrast, in the oceanic A domain, the 1D-Vz profiles of the basement do not match the profiles of either continental or typical oceanic crust (Figures 14 and 15b). Note that crustal architecture has similar velocity structure than oceanic crust defined by Watts *et al.*, (2009) in another segment of the Equatorial Atlantic Ocean (segment I in Figure 1): their wide-angle data present a thin layer with velocity 5.0 – 5.5 km/s overlying a high velocity layer of 7.0-7.2 km/s, with the Moho interpretation at circa 14-16 km.

Figure 16 presents several basement 1D-Vz profiles of intermediate domains of the South Atlantic margins and the western Mediterranean Sea, showing the evolution from an exhumed middle-lower continental crust to a thin oceanic crust. The Santos-São Paulo system (SSPS) (Figure 16a), offshore the southeast Brazilian margin, immediately north of the Florianópolis Fracture Zone, is interpreted as a kinematic buffer zone (Moulin *et al.*, 2012) and represents an entire conjugate passive margin system (Evain *et al.*, 2015). Whilst several studies have previously hypothesized the presence of either an aborted oceanic propagator (Mohriak, 2001; Mohriak and Szatmari, 2008; Mohriak *et al.,* 2010) or a failed spreading ridge (Demercian, 1996; Karner, 2000; Meisling *et al.*, 2001; Mohriak, 2001; Gomes *et al.*, 2002, 2009) in the SSPS surrounded by thinned continental crust, the acquisition of wide-angle seismic data has shown that the central part of the SSPS has never reached a typical oceanic crust (Evain *et al.*, 2015). Instead, in the central part of the SSPS, the southern profile of the Sanba survey shows 1D-Vz profiles that are very consistent with the surrounding domains and are interpreted as the result of exhumation of the middle/lower continental crust (green lines, Figure 16a) with two thinner crustal layers and a well-marked Moho. Only 50 km to the north, the northern wide-angle profile (yellow lines, Figure 16a) shows important lateral variations with the lack of the strong Moho step, replaced by a progressive increase in velocity in the lower layer, which can be interpreted as mantle intrusion or altered mantle (Evain *et al.*, 2015).

In the Jequitinhonha margin, the Salsa wide-angle experiment has shown that the typical oceanic crust is never imaged along two approximately 200-km-long profiles (Loureiro *et al.*, 2018) as shown on the 1D-Vz profiles (Figure 16b). Instead, this 150-km-wide transitional domain is interpreted as an exhumed lower continental crust with shearing of the deepest parts, underlain by an anomalous velocity zone. The seismic propagation velocities and geometry of the reflectors suggest the existence of a boudin-like feature probably linked to the crustal thinning, with an oceanward creep of the lower crust, or ultramafic intrusions in the lower crust (Loureiro *et al.*, 2018). Furthermore, the Provençal basin is a young, aborted rift system where both conjugate margins are accessible, with, in the central part, a domain assumed to be of oceanic nature (Burrus, 1984; Le Douaran *et al.*, 1984; De Voogd *et al.*, 1991; Pascal *et al.*, 1993; Rollet *et al.*, 2002; Gailler *et al.*, 2009) and characterized by a magnetic anomaly pattern that sharply differs from the quiet adjacent domains (Bayer et al., 1973; Galdéano and Rossignol, 1977) and a concomitant low-gravity anomaly. The Sardinia wide-angle experiment (Moulin *et al.*, 2015; Afilhado *et al.*, 2015) has shown the strong symmetrical segmentation of the basin, with intermediate domains on both sides interpreted as exhumed lower continental crust and a central part of the 4-5-km-thick atypical oceanic domain with strong variations between the conjugate profiles. Figure 16c presents the 1D-Vz profiles of the Gulf of Lion profile (purple lines) and the Sardinia profile (red lines). Whilst the comparison between the 1D velocity structure of typical oceanic crust (White *et al.*, 1992 and Christeson *et al.*, 2019) and the Sardinian 1D-Vz profiles shows a thinner crust consistent with oceanic crust (Afilhado *et al.*, 2015), the Gulf of Lion 1D-Vz profiles present strong similarities with the 1D-Vz profile of the adjacent domain interpreted as exhumed and intruded lower continental crust. As quoted by Afilhado *et al.* (2015), this observation raises the question as to the role of the lower continental crust "flow" which was maybe gradually recrystallized to build the first atypical oceanic crust (Bott, 1971; Aslanian *et al.*, 2009; Sibuet *et al.*, 2012). A similar evolution is observed on the segmentation of the Pará-Maranhão-Barreirinhas-Ceará segment from its Oceanic domain A to Oceanic domain B (Figure 14 & 16d).

Figure 17 compiles the evolution of the 1D-Vz profiles and compares them with new wide-angle and MCS seismic results acquired on the North Colorado margin (Shuck *et al.*, 2019; Becel *et al.*, 2020). The Colorado 1D-Vz profiles (black lines in Figure 17), between the two Magnetic anomalies ECMA (East Coast Magnetic Anomaly) and BSMA (Blake Spur Magnetic Anomaly), are interpreted as a proto-oceanic domain before the establishment of normal steady-state oceanic spreading ridge, which according to these authors started at the time of the Blake Spur with an approximate age of ≈170 Ma, which may correspond to a strong change in the spreading rates (an increase from ≈0.8 cm/y to ≈1.7 cm/y*)* and direction, from NNW–SSE to NW–SE (Sahabi *et al.*, 2004; Labails *et al.*, 2010) or an eastward ridge jump (Vogt, 1973; Bird *et al.*, 2007).

These 1D-Vz profiles present top velocities between 5.7 and 6 km/s, which are much higher than the velocity structure of a normal oceanic crust (figures 14 to 17 ; White *et al.*, 1992; Christeson *et al*., 2019). These 1D-Vz profiles fit better with the 1D-Vz profiles of the central part of the Santos Basin (green lines in Figures 16 & 17) or the 1D-Vz profiles of the Jequitinhonha Basin, with a smaller thickness. In these two basins, the sampled domain is interpreted as exhumed/intruded lower continental crust (Evain *et al.*, 2015; Loureiro *et al.*, 2018), which took place before the inset of true oceanic crust spreading.

For the evolution of the Central Atlantic margin, Becel *et al.* (2020) propose a new model in which the complete continental breakup of the conjugate margins system was delayed by a slow extension rate and finally achieved at Blake Spur Magnetic Anomaly time (early Bajocian), about 20 My after a first breakup at Sinumerian time (Sahabi *et al.*, 2004).

Further north, in the conjugate Mesozoic Tarfaya–Laayoune and George Bank basins system, Labails *et al.* (2009) highlighted strong asymmetry of this system for the first phases of seafloor accretion until the BSMA, which they attributed to the existence of the unaffected Precambrian Reguibat Craton on the African side: for these authors, the main thinning process seems to have occurred along the Baltimore Canyon margin and within the lower continental crust.

Toward*s* the north, a similar observation of asymmetrical process is observed: on the one hand, on the western margin, the SMART 1 Profile seems to show the presence of a thin continental crust above a layer of serpentinized mantle off the East Coast Magnetic Anomaly (Funck et al., 2004) while on the eastern conjugate margin, a true oceanic crust is interpreted on the MIRROR profile (Biari et al., 2015) off the conjugate West African Coast Magnetic Anomaly (Sahabi et al., 2004).

Whatever the nature of this American intermediate domain between the ECMA and the BSMA, asymmetry is visible, always on the same side and throughout the entire Central Atlantic Ocean, at least during the first phases of seafloor accretion.

It is problematic to define the difference between a proto-oceanic crust and exhumed/intruded lower continental crust, as short lateral variations may often occur in this mixing area as in the Santos Basin or the Provençal Basin, and it may become a subject of interminable debate. The evolution of 1D-Vz profiles every 10 km provides a favourable image of the evolution along one profile, with rather homogenous segments and strong velocity steps in between (see for instance Moulin *et al.*, 2015 or Aslanian *et al.*, 2021). As shown in the Provençal, Santos, Angola, Jequitinhonha and Pará-Maranhão-Barreirinhas-Ceará basins, the evolution from a passive margin towards a true oceanic crust was progressive, and probably involved the lower continental crust in the proto-oceanic crust construction, as previously suggested (Bott, 1971, Aslanian *et al.*, 2009; Sibuet *et al.*, 2012).

Contrary to Aslanian *et al.* (2009), who described a stress field that narrows by steps from more than 500 km to less than 50 km in the South Atlantic margins, Becel *et al.* (2020) claim that continental rifting between eastern North America and northwest Africa did not lead to rapid localization of extensional strain as previously thought. They suggest that the full continental breakup was delayed with apparent variations in the spreading rate of proto-oceanic crust possibly highlighting the continuous thermal erosion of the continental mantle lithosphere by mantle melts over time up until the formation of the BSMA. The pinch-out of continental mantle lithosphere at the apex of the end of the proto-oceanic crust in their model may correspond to the deep reflectors observed on the ION-GXT 7000 line, which also seem to pinch out at the apex of the inset of thin oceanic crust (Figure 13A).

8. Conjugate margin, asymmetry and age of the oldest oceanic crust

Any margin is only a part of the jigsaw, half part of a margins system, and palinspastic reconstructions are needed to understand the evolution of the entire jigsaw. Figure 18 presents a palinspastic reconstruction of the Brazilian-Ivory Coast-Ghana system at 100 Ma, with the Euler pole of Moulin et al. (2010). Due to the lack of magnetic information during this period, this position the position of the South American plate respect to African plate is extrapolated from the intermediate pole at C34 of Campan (1995) and the fit of Moulin *et al.* (2010) at 112 Ma, assuming a constant spreading rate. This extrapolation identifies a good fit between the small circles and the fracture zones, which indicates that no change in movement direction occurred between C34 and the fit, but the timing of the breakup remains unknown. If, as in the Central Atlantic Ocean, the rate of extension was low during the initial development of the continental rift (Labails *et al.*, 2010; Becel *et al.*, 2020), the reconstruction presented in Figure 18 is younger than 100Ma.

Knowing the exact position of the first proto-oceanic or oceanic crust on the African side, which would imply an asymmetric or symmetric system, is of major importance in understanding its evolution. Both supposed African oceanic limits from Heine et al. (2013) and Sage et al. (1997) are represented of Figure 18. Whatever the age of this reconstruction, as this margins system is strongly influenced by the NW-SE direction as demonstrated on the Brazilian side, the rounded shape and position of LALOC (Heine et al., 2013; Mueller et al., 2016) raises issues. Moreover, as the Brazilian side is now well constrained and described, this would imply a strong asymmetry between the two sides of the system. These issues are less significant but still present with the Continent-Ocean Boundary (COB) from Sage et al. (1997). Present knowledge and data do not provide the age of the first oceanic inset. We would need to conduct specific experiments on the Ghana-Ivory Coast margins to clarify this question. It is maybe worth to note that In contrast Figure 18 shows a striking coincidence to the alignment at that time (100Ma) of the Brazilian and African coasts and the inner limit of the Brazilian proto-oceanic crust.

9. Conclusion

The Pará-Maranhão-Barreirinhas-Cearà margin shows an E-W segmentation with, in the presumed oceanic crust, two different domains. Along the MC1 profile, which entirely crosses the margin, the first A domain appears homogeneous, with strong affinity with the deep basin interpreted as exhumed lower continental crust (Aslanian *et al.*, 2021). Further to comparison with similar studies in the Angola Margin (Aslanian *et al.*, 2009), the Provençal Basin (Moulin *et al.*, 2015; Afilhado *et al.*, 2015), the Santos Basin (Evain *et al.*, 2015), the Jequitinhonha Basin (Loureiro *et al.*, 2018) and the eastern North American Margin (Becel *et al.*, 2020), we interpret this domain as a proto-oceanic crust preceding the inset of true oceanic crust and following the inset of an exhumed/intruded middle/lower continental crust, following the idea of Bott (1971) and Aslanian *et al.* (2009).

As suggested by Becel *et al.* (2020), this evolution may suggest a continuous thermal erosion of the continental mantle lithosphere by mantle melts over time until the inset of true oceanic crust.

In 2009 and 2018, Aslanian *et al.* highlighted the crucial role of the lower continental crust and mantle intrusions in the passive margin formation and proposed an evolution in three stages: 1) a first rift stage, with small or no crustal thinning but mafic intrusions which produced overloading and subsidence (Tozer *et al.*, 2017; Shulgin *et al.*, 2018; Moulin *et al.*, 2020; Leprêtre *et al.*, 2021); 2) an exhumation phase, which is the main thinning phase and produces a basement made of exhumed/intruded lower continental crust, proto-oceanic crust (Contrucci *et al.*, 2004; Funck *et al.*, 2004; Moulin *et al.*, 2005; Aslanian and Moulin, 2012; Sibuet *et al.*, 2012; Moulin *et al.*, 2015; Afilhado *et al.*, 2015; Evain *et al.*, 2015; Loureiro *et al.*, 2018; Shuck *et al.*, 2019; Becel *et al.*, 2020), and in some rare cases, exhumed mantle (e.g., Péron-Pinvidic and Manatschal, 2008); and 3) the oceanic spreading stage. This scheme may be progressive, with lower continental material flow inside a first proto-oceanic crust and as suggested by Becel *et al.* (2020) continental mantle lithosphere erosion before the inset of true oceanic crust.

Acknowledgements

The authors wish to thank the captain, officers and crew of the R/V. Pourquoi Pas?, together with the OBS teams of Ifremer (J. Crozon, P. Pelleau, M. Roudaut, R. Apprioual, D. Le Piver & P. Fernagu), IUEM (C. Prunier), who operated the Ifremer – IUEM seabed instruments during the MAGIC cruise. Land-based assistance was provided by IDL (Portugal) (A. Loureiro, C. Corela, J-L. Duarte, I. Bernardo, D. Alves) and Univ. of Brasilia (Brazil) (J. Soares, M. V. de Lima) in Brazil who operated instruments from the ON pool. We also thank the MAGIC scientific team (F. Klingelhoefer, M. Benabdellouahed, A. Baltzer, M. Rabineau, Z. Mokeddem, E. Boisson, F. Farias, R. Pellen, B. Pereira, C. Rigoti) who took part in the data acquisition and contributed to the good spirit of the mission.

This research was funded by Petrobras and Ifremer. R. Fuck acknowledges CNPq research fellowship. The authors acknowledge financial support from CAPES-COFECUB. The GMT version 5, Zelt, and Seismic Unix software packages (Wessel et al., 2011; Zelt and Smith, 1992 and Cohen and Stockwell, 2003 respectively) were used to create some of the figures.

The authors acknowledge the fruitful and constructive English editing advices and corrections by Alison Chalm.

We would also like to thank the chief editor, Francisco J Vega, and Michelangelo Martini and another anonymous reviewer for their constructive and detailed reviews, which greatly improved the manuscript.

Author contributions

The MAGIC Project was imagined by D. Aslanian and led by D. Aslanian, M. Moulin from Ifremer and A. Viana, O. da Cruz Pessoa Neto from Petrobras. The onshore part of the project was managed by N. Dias from ISEL (Lisbon), R. Fuck and J. Soares from University of Brasilia. Modelling of the MAGIC profiles was performed by M. Moulin, F. Gallais, A. Afilhado and P. Schnurle. Processing of deep seismic reflection data was performed by P. Schnurle. Geologic interpretation was performed by M. Moulin, D. Aslanian, P. Schnürle, F. Gallais, A. Afilhado and M. Evain. All co-authors participated in writing the paper. The MAGIC Team is composed of: A. Baltzer[6], M. Rabineau[7], Z. Mokkedem[7], M. Benabdelhouahed[7], A. Loureiro[3], D. Alves[3], F. Klingelhoefer[1], R. Apprioual[1], J. Crozon[1], P. Fernagu[1], D. Le Piver[1], P. Pelleau[1], C. Prunier[7], M. Roudaut[1], L. Morvan[1], D. Pierre[1], E. Boisson[1], M. Roudaut-Pitel[1], I. Bernardo[3], C. Corela[3], J.L. Duarte[3], M. De Lima[8], L. Matias[3], F. Farias[5], R. Pellen[1,6], B. Pereira[5], C. Rigoti[5] & W. Roest[1]. The dataset collected during the MAGIC experiment is protected under a partnership with Petrobras. Any request has to be addressed to Daniel Aslanian (aslanian@ifremer.fr) and Adriano Viana (aviana@petrobras.com.br).

Figures

Figure 1: a) Kinematic reconstruction at C34 (Campanian, 84 Ma) of the Equatorial Atlantic Ocean, after Moulin et al. (2010), showing segmentation of the Equatorial Segment and localisation of Figures 1b and 2a. The figure shows, on each plate, the gravity data from Sandwell and Smith (1997) between the coast and the anomaly C34. The West African plate is fixed. b) Bathymetry map of the Pará-Maranhão/Barreirinhas margin acquired during the MAGIC experiment. White circles represent the OBS deployed during the MAGIC experiment. GXT lines are indicated by dotted red lines and labels. Blue rectangle shows the location of the OBS presented in this study. Location of basin I, II and volcanic alignment, issued from Aslanian et al., 2021 is also indicated.

Figure 2: a) Gravity map of the Ghana-Ivory Coast margin, see general location in Figure 1a. The position of kinematic fit from Moulin et al. (2010) is in blue. The dotted red line represents the supposed True Oceanic Boundary resulting from refraction studies (Pierce et al., 1996; Sage et al., 1997; Edwards et al., 1997) whilst the pink line represents the position of Landward Limit Oceanic Crust from Heine et al. (2013). Positions of the Equasis, Equaref and Darwin cruise 55 experiments and some industrial lines available are in black; thick yellow lines represent the part of the profiles shown in Figure 2b. White dots represent the

OBS, which register data. Brown area represents the West African craton. b) Final velocity model of 2 seismic lines located on the Ivory Coast Basin (yellow lines on the map below) from Pierce et al. (1996, EQUARE-1) and Sage (1994, EQUAREF-7). The basement and the Moho are indicated by thick black lines, the anomalous velocity zone of EQUAREF-1 profile by a thick red line, and the supposed oceanic crust by a blue area. The positions of the landward Limit Oceanic Crust from Heine et al. (2013) and the fit from Moulin et al. (2010) are also indicated by pink and blue lines, respectively.

Figure 3: Comparison between MC1OBS06, MC1OBS12 and MC1OBS24 on the MAGIC1 profile – southeast direction to the right and northwest to the left. a) Colour-coded observed travel-times reduced by a velocity of 4 km/s overlain by predicted times in black. b) Seismic rays. c) MCS time migrated section and colour-coded model interfaces.

Figure 4: MC1OBS09 on the MAGIC1 profile – southeast direction to the right and northwest to the left. a) Seismic record. b) Synthetics. c) Colour-coded synthetics. d) Colour-coded observed travel-times overlain by predicted times in black. e) Corresponding ray tracing of black line in Figure 4d. f) MCS time migrated section and colour-coded model interfaces. On a, b, c, and d, travel-time is reduced by a velocity of 7 km/s. Same legend and colour code as Figure 3.

Figure 5: MC1OBS11 on the MC1 profile - southeast direction to the right and northwest to the left. Same legend and colour code as Figure 3.

Figure 6: MC1OBS18 on the MC1 profile - southeast direction to the right and northwest to the left. Same legend and colour code as Figure 3. Note that the horizontal scale of this profile is different from the previous one.
Figure 7: MC1OBS24 on the MC1 profile - southeast direction to the right and northwest to the left. Same legend and colour code as Figure 3.

Figure 8: Velocity model of the MC1 profile. Thick black lines mark layer boundaries from the modelling. Coloured areas are constrained by seismic rays. Inverted black triangles mark OBS positions and thin blue lines cross points with other MAGIC profiles and the ION-GXT profiles. Vertical exaggeration 1:5. Thin blue lines mark the intersection with MAGIC and ION-GXT datasets.

Figure 9: Gravity model for the MAGIC1 profile overlain by interfaces from wide-angle modelling. a) Density model up to a depth of 30 km. b) Free-air gravity anomaly observed (Pis et al., 2012) along the MAGIC1 profile (red dotted) and calculated (black line). c) Load anomaly.

Figure 10: a) Distribution of interface depth nodes and top and bottom velocity nodes of the final P-wave interval velocity model along the MAGIC1 wide-angle profile. Interfaces where reflections have been observed on OBS data are highlighted in blue. b) Hit count of rays traced in the model during inversion. Depth interface nodes are plotted with squares scaled to the hit count through the node. c) Spread-Point Function (SPF) in the model. Depth interface nodes are plotted with squares scaled to the SPF at the node. d) Resolution in the model. Depth interface nodes are plotted with squares scaled to the resolution at the node.

Figure 11: Two-way travel-time record section of MCS data along the MAGIC1 profile A) un-interpreted and B) overlain by time-converted interfaces of the wide-angle model. Intersections with MAGIC and ION-GXT datasets are indicated by red and grey arrows, respectively. OBS locations are indicated in blue at the base of the profile. Vertical exaggeration at seafloor is 1:12.5.

Figure 12: Pre-stack depth migrated record section of MCS data along the MAGIC1 profile

A) un-interpreted and B) Model's interfaces are represented with continuous lines. Intersections with MAGIC and ION-GXT datasets are indicated by red and grey arrows, respectively. Vertical exaggeration is 1:5.

Figure 13*: A) Line drawing of the depth-converted profile ION-GXT 7000, coincident with the MC3 profile (Aslanian et al., 2021). Thick blue lines indicate where wide-angle reflections hit the interface. B) MC3OBS11 (indicated in blue triangle in figure 13A) on the MAGIC3 profile – east direction to the right and west to the left. a) Seismic record; b) Synthetics; c) Colour-coded synthetics; d) Colour-coded observed travel-times overlain by predicted times in black; e) Seismic rays; f) MCS time migrated section and colour-coded model interfaces. On a, b, c, and d, travel-time is reduced by a velocity of 7 km/s.*

Figure 14*: a) Distribution of 1D- velocity/depth profiles extracted every 10 km from part of the final P-wave velocity model showing the segmentation (colour code in legend) along MC4 (a - top), MC2 (b - middle) and MC3 (c - bottom) profiles, crossing Basins IIA and I and the presumed oceanic crust. Velocity profiles for oceanic crust are a compilation of White et al., 1992 (black lines) and Christeson et al., 2019 (orange lines). Grey area on profiles indicates the High Velocity Layer (H.V.L.) revealing by Aslanian et al., 2021.*

Figure 15*: Top: Total 1D-VZ profile (including water and sediment layers) of the three crossing points between the MC1 profile and the MC2, MC3 and MC4 profiles, within the presumed oceanic A domain. Bottom: distribution of 1D- velocity/depth profiles extracted every 10 km from part of the final P-wave velocity model showing the segmentation (colour code in legend) along MC1, crossing the supposed oceanic domain. Light Purple area: compilation of velocity profiles for the oceanic crust (White et al., 1992 and Christeson et al., 2019).*

Figure 16*: Compilations of the Basement 1D-Vz profiles extracted every 10 km. Light grey area: compilation of velocity profiles for the oceanic crust (White et al., 1992 and Christeson et al., 2019). a) SANBA experiment – the central part of the Santos-São Paulo system: Green: south profile; Yellow: north profile (Evain et al., 2015); b) SALSA experiment: deep basin of the Jequitinhonha margin in orange (Loureiro et al., 2018); c) SARDINIA experiment in the Provençal Basin: evolution from the proto-oceanic crust of the Gulf of Lion (purple, Moulin et al., 2015) to the thin oceanic crust (red, Afilhado et al., 2015) on the Sardinian side; D) MAGIC experiment: proto-oceanic crust (purple) and thin oceanic crust (red) (This study).*

Figure 17*: Compilation of the Basement 1D-Vz profiles of figure 17 (with the same colour code) and the Basement 1D-Vz profiles of the Colorado Basin (Shuck et al., 2019).*

Figure 18*: Palinspastic reconstruction of the Pará-Maranhão/Barreirinhas—Ghana-Ivory Coast system. Euler pole from Moulin et al. (2010). The south American plate is fixed. Note that, due to the lack of magnetic information during this period, this position is extrapolated from the intermediate pole at C34 of Campan (1995) and the fit of Moulin et al. (2010) at 112 Ma, with a constant and regular spreading rate. The segmentation of the Pará-Maranhão/Barreirinhas margin issued from this study and Aslanian et al. (2021) (in blue lines) is represented together with the location of the LaLOC, the African COB from Sage et al. (1997) and different propositions for the initial fit (Moulin et al., 2010 ; Heine et al., 2013 and Muller et al., 2016)*

References

Afilhado, A. Moulin, M., Aslanian, D., Schnürle, P., Klingelhoefer, F., Rabineau, M., Leroux, E., Beslier, M.-O., 2015. Deep Crustal Structure Across An Young Passive Margin From Wide-

Angle And Reflection Seismic Data (The Sardinia Experiment) - II: Sardinia's Margin, *Bulletin de la Société Géologique de France*, 186, n°4-5, 331-351, doi:10.2113/gssgfbull.186.4-5.331.

Antobreh, A.A., Faleide, J.I, Tsikalas, F.T and Planke, S., 2009. Rift–shear architecture and tectonic development of the Ghana margin deduced from multichannel seismic reflection and potential field data, *Marine and Petroleum Geology,* 26, 3, 345-368.

Aslanian, D., Moulin, M., Olivet, J-L., Unternehr, P., Bache, F., Rabineau, M., Matias, L., Nouzé, H., Klingelhoefer, F., Contrucci, I. and Labails, C., 2009. Brazilian and African passive margins of the Central Segment of the South Atlantic Ocean: kinematic constraints, *Tectonophysics*, 468, 98-112.

Aslanian, D. & Moulin, M., 2010. Comments On "A New Scheme For The Opening Of The South Atlantic Ocean And The Dissection Of An Aptian Salt Basin" From Torsvik *et al.*, *Geophys. J. Int.*, Doi: 10.1111/J.1365-246x.2010.04727.X

Aslanian, D. & Moulin, M., 2012. Paleogeographic consequences of conservational models in the South Atlantic Ocean, *In*: Mohriak, W.U., Danforth, A., Post, P.J., Brown, D.E., Tari, G.C., Nemcok, M. & Sinha, S.T. (*eds*). Conjugate Divergent Margins. *Geological Society, London, Special Publications*, 369, http://dx.doi.org/10.1144/SP369.5,

Aslanian, D., Moulin, M., Schnürle, P., Evain, M., Afilhado, A., & Rabineau, M. (2018). Passive margin and continental basin: Towards a new paradigm, 1ere Conference of the Arabian Journal of Geosciences (CAJG), 12–15 November 2018, Hammamet, Tunisia.

Aslanian, D., Gallais, F., Afilhado, A., Schnurle, P., Moulin, M., Evain, M., Dias, N., Soares, J., Fuck, R., da Cruz Pessoa Neto, O., Cupertino, J.A., Viana, A. and the MAGIC Team, Deep structure of the Pará Maranhão/Barreirinhas passive margin in the Equatorial Atlantic (NE Brazil), accepted to *Journal of South American Earth Sciences*.

Auffret Y., Pelleau P., Klingelhoefer F., Géli L., Crozon J., Lin J.I., Sibuet J.-C.**,** 2004. MicrOBS : a new generation of bottom seismometer, *First Break*, **22**, 41-47.

Austin Jr, J. A. & Uchupi, E., 1982, Continental-Oceanic Crustal Transition Off Southwest Africa, *Am. Assoc. Pet. Geol. Bull.*, 66, 1328-1347.

Azevedo, R.P., 1991. Interpretation of a Deep Seismic Reflection Profile in the Pará- Maranhão Basin. *Congresso Brasileiro de Geofísica, 2, Bol. Res. Exp., Salvador, BA, II, SBGF*, Salvador, BA: 661–666.

Basile C, Mascle J, Popoff M, Bouillin JP, Mascle G, 1993. The Ivory Coast-Ghana transform margin: a marginal ridge structure deduced from seismic data. *Tectonophysics*, 222, 1–19

Basile, C., Mascle, J. and Guiraud, R., 2005. Phanerozoic geological evolution of the Equatorial Atlantic domain. *Journal of African Earth Sciences*, 43: 275–282.

Bayer R., Le Mouël J.-L. & Le Pichon X., 1973. Magnetic anomaly pattern in the western Mediterranean. *Earth Mlanet. Sci. Lett.*, 19, (2), 168-176.

Bécel, A., Davis, J. K., Shuck, B. D., Van Avendonk, H. J. A., & Gibson, J. C., 2020. Evidence for a prolonged continental breakup resulting from slow extension rates at the eastern north American volcanic rifted margin. *Journal of Geophysical Research: SolidEarth*, 125, e2020JB020093. https://doi.org/10.1029/2020JB020093, Biari, Y., F.Klingelhoefer, F., Sahabi, M., Aslanian, D., Schnurle, P., Berglar, K., Moulin, M., Mehdi, K., Graindorge, D., Evain, M., Benabellouahed, M. & Reichert, C., 2015, Deep crustal structure of the north-west African margin from combined wide-angle and reflection seismic data (MIRROR seismic survey), *Tectonophysics*, 656, 154–174, doi:10.1016/j.tecto.2015.06.019.

Bird, D.E., Hall, S.A., Burke, K., Casey, J.F., Sawyer, D.S., 2007. Early Central At-lantic Ocean seafloor spreading history. Geosphere3, 282–298. https://doi .org /10 .1130 /GES00047.1.

Blarez, E., 1986. Structure Et Évolution D'une Marge Continentale Transformante. Thèse De Doctorat, *Univ. Pierre Et Marie Curie*, Paris, 188 Pp.

Bott, M.H.P., 1971. Evolution of young continental margins and formation of shelf basin. *Tectonophysics* **11**, 319**–**337.

Burrus J., 1984, Contribution to a geodynamic synthesis of the Provencal basin (northwestern Mediterranean). *Mar. Geol.,* **55***,* 247-269.

Campan, A., 1995. Analyse Cinématique De L'atlantique Equatorial , Implications Sur L'évolution De L'atlantique Sud Et Sur La Frontière De Plaque Amérique Du Nord/Amérique Du Sud. Thèse De Doctorat, *Univ. « Pierre Et Marie Curie »*, Paris Vi, 352 Pp.

Canales J. P., Tucholke, B. E., Xu, M., Collins, J. A. & DuBois, D. L., 2009. Seismic evidence for large-scale compositional heterogeneity of oceanic core complexes, *G3*, **9**, Q08002, doi:10.1029/2008GC002009

Carton, H., S. C. Singh, N. D. Hananto, J. Martin, Y. S. Djajadihardja, Udrekh, D. Franke, and C. Gaedicke., 2014. Deep seismic reflection images of theWharton Basin oceanic crust and uppermostmantle offshore Northern Sumatra: Relation with active and past deformation, J. Geophys. Res. Solid Earth, 119, 32–51, doi:10.1002/2013JB010291.

Christeson, G.L., Goff, J.A. and Reece R.S., 2019. Synthesis of oceanic crustal structure from two□dimensional seismic profiles. *Reviews of Geophysics*, 57, 504–529. https://doi.org/10.1029/2019RG000641.

Cohen, J.K. & Stockwell, J.W., 2003. Seismic Unix Release 37: A free package for seismic research and processing. Center for Wave Phenomena, Colorado School of Mines.

Contrucci, I., L. Matias, M. Moulin, L. Géli, F. Klingelhoeffer, H. Nouzé, D. Aslanian, J-L. Olivet, J-C. Sibuet and J.-P. Réhault, 2004. Deep structure of the West African continental margin, between 5°S and 8°S, from reflexion / refraction seismics and gravity data, *Geophys. J. Int*, 158: 529-553, DOI: 10.1111/j.1365-246X.2004.02303.x.

Curie, D., 1984. Ouverture De L'atlantique Sud Et Discontinuités Intra-Plaque : Une Nouvelle Analyse. Thèse 3ème Cycle, *Univ. De Bretagne Occidentale*, Brest, 192 Pp.

De Voogd B., Nicolich R., Olivet J.-L., Fanucci F., Burrus J., Mauffret A., Pascal G., Argnani A., Auzende J.-M., Bernabini M., Bois C., Carmignani L., Fabbri A., Finetti I., Galdeano A., Gorini C.Y., Labaume P., Lajat D., Patriat P., Pinet B., Ravat J., Ricci Luchi F. & Vernassa S. 1991. First deep seismic reflection transect from the Gulf of Lions to Sardinia (ECORS-CROP profiles in western Mediterranean). *In*: R. Meissner, L. Brown, H.-J. Durbaum, K. Fuchs and F. Seifert, Eds., Continental lithosphere: deep seismic reflections. American Geophysical Union, *Geodynamics*, **22**, Washington, 265-274.

Demercian, L. S. 1996. A halocinese na evolucao do Sul da Bacia de Santos do Aptiano ao Creta´ceo Superior. Master's thesis, Universidade Federal do Rio Grande do Sul, Porto Alegre, Brazil.

Edwards, R.A, Whitmarsh, R. B. & Scrutton, R. A., 1997. Synthesis of the crustal structure of the transform continental margin off Ghana, northern Gulf of Guinea, *Geo-Marine Letters*, **17**, 12-20.

Evain M., Afilhado, A., Rigotti, C., Loureiro, A., Alves, D., Klingelhoefer, K., Schnürle, P., Feld, A., Fuck, R., Soares, J., Vinicius de Lima, M., Corela, C., Matias, L., Benabdellouahed, M., Baltzer, A., Rabineau, M.,Viana, A., Moulin, M., Aslanian, D., 2015): Deep structure of the Santos Basin-São Paulo Plateau System, SE Brazil, *J. of Geophy. Res. - Solid earth*, doi:10.1002/2014JB011561.

Funck, T., H. R. Jackson, K. E. Louden, S. A. Dehler, and Y. Wu (2004), Crustal structure of the northern Nova Scotia rifted continental margin (eastern Canada), J. Geophys. Res., 109, B09102, doi:10.1029/2004JB003008.

Gailler A., Klingelhoefer F., Olivet J.-L., Aslanian D. and the Sardinia scientific and technical OBS teams, 2009. Crustal structure of a young margin pair: New results across the Liguro –Provencal basin from wide-angle seismic tomography. *Earth Planet. Sci. Lett.*, **286**, 333-345.

Galdeano A. & Rossignol J.-C., 1977. Assemblage à altitude constante des cartes d'anomalies magnétiques couvrant l'ensemble du bassin occidental de la Mediterraneée.. *Bull. Soc. géol. Fr.*, 7, XIX, 461-468.

Gomes, P. O., Kilsdonk, B., Minken, J., Grow, T. & Barragan, R. 2009. The outer high of the Santos Basin, Southern Sa˜o Paulo Plateau, Brazil: pre-salt exploration outbreak, paleogeographic setting, and evolution of the syn-rift structures. In: AAPG International Conference and Exhibition, Cape Town, South Africa, October 26–29, 2008, Abstracts CD. http://www.searchanddiscovery.net/documents/2009/ 10193gomes/images/gomes.pdf (last accessed 2011

Gomes, P. O., Parry, J. & Martins, W. 2002. The outer high of the Santos Basin, southern Sao Paulo Plateau, Brazil: tectonic setting, relation to volcanic events and some comments on hydrocarbon potential. In: AAPG Hedberg Conference on the Hydrocarbon Habitat of Volcanic Rifted Passive Margins, September 8–11, Stavanger, Norway, Search and Discovery, Article 90022.

Gouyet, S., 1988. Evolution Tectono-Sédimentaire Des Marges Guyanaises Et Nord-Brésilienne Au Cours De L'ouverture De L'atlantique Sud. Thèse De Doctorat, *Univ. De Pau Et Des Pays De L'adour*, Pau, 374 Pp.Granot, R. and Dyment, J., 2015, The Cretaceous opening of the South Atlantic Ocean. *Earth and Planetary Science Letters*,414, 156–163, http://dx.doi.org/10.1016/j.epsl.2015.01.015

Granot, R. and Dyment, J., 2015. The Cretaceous opening of the South Atlantic Ocean. *Earth and Planetary Science Letters,* 414, 156–163.

Heine, C., Zoethout, J., Mueller, R. D., 2013. Kinematics Of The South Atlantic Rift, *Solid Earth*, 4, 2, 215-253.

Karner, G. D. 2000. Rifts of the campos and Santos Basins, Southeastern Brazil: distribution and timing. In: Mello, M. R. & Katz, B. J. (eds) Petroleum Systems of South Atlantic Margins. *AAPG, Memoirs*, 73, 301–315.

Labails, C., Olivet, J.-L., and the “Dakhla group” (between them **Moulin, M.**), (**2009**). Crustal Structure of the SW-Morrocan margin (Dakhla experiment). Part B - the tectonic heritage *Tectonophysics* (Special Issue: role of magmatism), 468: 83-97, doi:10.1016/j.tecto.2008.08.028

Labails, C., J.-L. Olivet, D. Aslanian, and W. R. Roest, 2010, An alternative early opening scenario for the central Atlantic Ocean,Earth Planet.Sci. Lett., 297, 355–368, doi:10.1016/j.epsl.2010.06.024.

Le Douaran S., Burrus J. & Avedik F., 1984, Deep structure of the northwestern Mediterranean basin: results of a two-ship seismic survey. *Mar. Geol.*, **55**, 325-345.

Leprêtre, A., Schnürle, P., Evain, M., Verrier, F., Moocroft, D., de Clarens, P., Corela, C., Afilhado, A., Loureiro, A., Leroy, S., d'Acremont, E., Thompson, J., Aslanian, D. and Moulin, M., Deep structure of the North Natal Valley (Mozambique) using combined wide-angle and reflection seismic data, ***accepted to JGR***

Leroux L., Aslanian D., Rabineau M., Moulin M., Pellen R., 2018. The late Messinian event: a worldwide tectonic revolution. Terra Nova, 30(3), 207-214. Publisher's official version : https://doi.org/10.1111/ter.12327 , Open Access version : https://archimer.ifremer.fr/doc/00422/53362/

Liu, Z. & Bleistein, N., 1995. Migration velocity analysis: theory and an iterative algorithm, *Geophysics*, 60, 142-153.

Loureiro, A., Schnürle, P., Klingelhöfer, F., Afilhado, A., Pinheiro, J., Evain, M., Gallais, F., Dias, N., Rabineau, M., Baltzer, A., Benabdellouahed, M., Soares, J., Fuck, R., Cupertino, J. A., Viana, A., Matias, L., Moulin, M., Aslanian, D. & SALSA team. 2018. Imaging exhumed lower continental crust in the distal Jequitinhonha basin, Brazil. *Journal of South American Earth Sciences*, 84, 351-372 http://doi.org/10.1016/j.jsames.2018.01.009

Ludwig, W.J., Nafe, J.E., Drake, L.E., 1970. Seismic refraction. In: In: Maxwell, A.E. (Ed.), The Sea. New Concepts of Sea Floor Evolution, vol. 4. Wiley-Interscience, New York, 53–84.

Lutter W. J., and R. L. Nowack, 1990. Inversion for crustal structure using reflections of the PASSCAL Ouachita experiment, Geophysical Journal International, 95, 4633-4646.

Mascle, J. & Blarez, E., 1987. Evidence for transform margin evolution from the Ivory-Ghana continental margin, Nature, 326, 378-381.

Mascle, J. Basile, C., Pontoise, B. & Sage, F., 1995. The Cote d’Ivoire – Ghana transform margin: an example of the ocean-continent transform boundary, *Kluwer-NATO Book*, Special Volume on Rifted Ocean Continent Boundaries E. Banda , M. Talwany and M. Torné (Eds), 327-339.

Mascle, J., Lohmann, G.P., Moullade, M., 1988. *Proc. ODP, Sci. Results*, 159: College Station, TX (Ocean Drilling Program).

Matos, R. M. D. 1992. The northeast Brazilian rift system. *Tectonics*, 11, 766–791.

Meisling, K. E., Cobbold, P. R. & Mount, V. S. 2001. Segmentation of an obliquely rifted margin, Campos and Santos basins, southeastern Brazil. *AAPG Bulletin*, 85, 1903–1924.

Mohriak, W.U., 2001. Salt Tectonics, Volcanic Centers, Fracture Zones And Their Relationship With

The Origin And Evolution Of The South Atlantic Ocean: Geophysical Evidence In The Brazilian And West African Margins. 7Th International Congress Of The Brazilian Geophysical Society, Salvador - Bahia - Brazil, October 28-31, 2001, Expanded Abstract, P. 1594.

Mohriak, W. U. & Szatmari, P. 2008. Tectônica de Sal. In: Mohriak, W. U., Szatmari, P.&dos Anjos, S.M. (eds) Sal, Geologia e Tectônica, exemplos nas bacia brasileiras. Beca Edic¸o˜es Ltda, Sa˜o Paulo, 90–163.

Mohriak, W. U., Nobrega, M., Odegard, M. E., Gomes, B. S. & Dickson, W. G. 2010. Geological and geophysical interpretation of the Rio Grande Rise, southeastern Brazilian margin: extensional tectonics and rifting of continental and oceanic crusts. *Petroleum Geoscience*, 16, 231–245, doi: 10.1144/1354-079309-910.

Moulin, M., D. Aslanian, J-L. Olivet, I. Contrucci, L. Matias, L. Géli, F. Klingelhoeffer, H. Nouzé, Réhault, J.-P. and Unternehr, P., 2005. Geological constraints on the evolution of the angolan margin based on reflection and refraction seismic data (ZaïAngo project), *Geophys. J. Int.*, 162: 793-810, DOI: 10.1111/j.1365-246X.2005.02668,x.

Moulin, M., D. Aslanian, & Unternehr, P., 2010a, A New Starting Point For The South And Equatorial Atlantic Ocean, *Earth-Science Rev.*, 98, 1-37, Doi:10.1016/J.Earscirev.2009.08.001.

Moulin, M., Aslanian, D. 2010., Corrigendum to: A new starting point for the South and Equatorial Atlantic Ocean, Earth Sciences Reviews .

Moulin, M., Aslanian, D., Rabineau, M., Patriat M., &Matias, L., Kinematic Keys of the Santos – Namibe Basins, In: Mohriak, W.U., Danforth, A., Post, P.J., Brown, D.E., Tari, G.C., Nemcok, M. & Sinha, S.T. (eds). Conjugate Divergent Margins. *Geological Society, London, Special Publications*, 369, http://dx.doi.org/10.1144/SP369.3. 2012

Moulin, M., Klingelhoefer, F., Afilhado, A., Aslanian, D., Schnürle, P., Nouzé, H., Rabineau, M., Beslier, M.-O. & Feld A., 2015. Deep Crustal Structure Across An Young Passive Margin From Wide- Angle And Reflection Seismic Data (The Sardinia Experiment) - I. Gulf Of Lion's Margin, *Bulletin de la Société Géologique de France*, 186, n°4-5, 309- 330, doi:10.2113/gssgfbull.186.4-5.309.

Moulin, M., Aslanian, D., Evain, M., Leprêtre, A., Schnurle, P., Verrier, F., Thompson, J., De Clarens, P., Leroy, S., Dias, N. and PAMELA-MOZ35 Team, **2019**. Gondwana breakup: messages from the North Natal Valley, *Terra Nova*.

Müller, R.D., Seton, M., Zahirovic, S., Williams, S.E., Matthews, K.J., Wright, N.M., Shephard, G.E., Maloney, K.T., Barnett-Moore, N., Hosseinpour, M., Bower, D.J. & Cannon, J. 2016. Ocean Basin Evolution and Global-Scale Plate Reorganization Events Since Pangea Breakup, *Annual Review of Earth and Planetary Sciences*, 44, pp. 107 . DOI: 10.1146/annurev-earth-060115-012211.

Nedimovic, M.R., Carbotte, S., Harding, A., Detrick, R., Canles, J.P., Diebold, J., Kent, G., Tischer, M. & Babcock, J., 2005. Frozen magma lenses below the oceanic crust. *Nature*, 436, 1149-1152, doi10.1038/nature03944.

Oliveira Marinho, M., 1985. Le Plateau Marginal De Guinée : Transition Entre Atlantique Central Et Atlantique Equatorial. Thèse De Doctorat, *Univ. Pierre Et Marie Curie*, Paris Vi, 183 Pp.

Pascal, G.P., Mauffret, A., Patriat, P., 1993. The ocean–continent boundary in the Gulf of Lion from analysis of expanding spread profiles and gravity modeling, *Geophysical Journal International*, **113**, 701–726.

Pavlis, N.K., Holmes, S.A., Kenyon, S.C. & Factor, J.K., 2012. The development and evaluation of the Earth Gravitational Model 2008 (EGM2008). *Journal of Geophysical Research*, **117**, B04406, doi:04410.01029/02011JB008916.

Péron-Pinvidic, G., And G. Manatschal, 2008, The Final Rifting Evolution At Deep Magma-Poor Passive Margins From Iberia-Newfoundland: A New Point Of View, Int. J. Earth Sci., 98(7), 1581-1597, Doi:10.1007/S00531-008-0337-9.

Pierce, C., Whitmarsh, R.B., Scrutton, R.A., Pontoise, B., Sage, F. and Mascle, J., 1996. Côte d'Ivoire-Ghana margin: seismic imaging of passive rifted crust adjacent to a transform continental margin. *Geophysical Journal International*, 125, 781-795.

Rabinowitz, P. D. & Labrecque, J., 1979. The Mesozoic South Atlantic Ocean And Evolution Of Its Continental Margins. *Journal Of Geophysical Research*, 84: 5973-6002.

Rollet N., Déverchère J., Beslier M.-O., Guennoc P., Réhault J.-P., Sosson M. & Truffert C., 2002. Back arc extension, tectonic inheritance and volcanism in the Ligurian Sea, western Mediterranean. *Tectonics*, **21**, doi: 10.1029/2001TC900027.

Sage, F., 1994. Structure crustale d’une marge transformante et du domaine océanique adjacent : exemple de la marge de côte d’ivoire-ghana. Thèse de doctorat de l’Université de Pierre et Marie Curie, Paris 6, 404 pp.

Sage, F., Pontoise, B., Mascle, J., Basile, C., Arnould, L., 1997. Crustal structure and ocean- continent transition at marginal ridge: the Côte d'Ivoire–Ghana marginal ridge. *Geo-Mar. Lett.*, 17, 40–48.

Sahabi, M., Aslanian, D. & Olivet, J.-L., 2004. Un nouveau point de départ pour l'histoire de l'Atlantique Central. *Compte Rendus Geosciences*, **33**: 1041-1052.

Sandwell, D.T. & Smith, W.H.F., 1997. Marine gravity anomaly from Geosat and ERS-1 satellite altimetry. *Journal of Geophysical Research,* 102**,** 803–827.

Sauter, D., Ringenbach, J. C., Cannat, M., Maurin, T., Manatschal, G., &McDermott, K. G. 2018. Intraplate deformation of oceanic crust in the West Somali Basin: Insights from long-offset reflection seismic data. *Tectonics*, 37, 588–603. https://doi.org/10.1002/2017TC004700

Sauter, D., Unternehr, P., Manatschal, G., Tugend, J., Cannat, M., Le Quellec, P., Kusznir, N., Munschy, M., Leroy, S., Mercier de Lepinay, J., Granath, J. W. & Horn, B.W., 2016, Evidence for magma entrapment below oceanic crust from deep seismic reflections in the Western Somali Basin. *Geology*, 44, 6, 407-410, doi:10.1130/G37747.

Shuck, B.D., VanAvendonk, H., J.,A., Becel, A., 2019. The role of mantle melts in the transition from rifting to seafloor spreading offshore eastern North America. *Earth and Planetary Science Letters*, 525, 115756, https://doi.org/10.1016/j.epsl.2019.115756

Shulgin, A., Mjelde, R., Faleide, J. I., Hoy, T., Flueh, E., & Thybo, H. (2018). The crustal structure in the transition zone between the western and eastern Barents Sea. *Geophysical Journal International*, *214*, 315–330. https ://doi.org/10.1093/gji/ggy139

Sibuet, J.-C. & Tucholke, B., 2012. The Geodynamic Province of Transitional Lithosphere Adjacent to

Magma-Poor Continental Margins. *In*: Mohriak, W.U., Danforth, A., Post, P.J., Brown, D.E., Tari, G.C., Nemcok, M. & Sinha, S.T. (*eds*). Conjugate Divergent Margins. *Geological Society, London, Special Publications*, 369, doi 10.1144/SP369.15.

Torsvik, T. H., S. Rousse, C. Labails, And M. A. Smethurst, 2009, A New Scheme For The Opening Of The South Atlantic Ocean And The Dissection Of An Aptian Salt Basin, *Geophys. J. Int.*, 177, 1315-1333, Doi:10.1111/J.1365-246x.2009.04137.X.

Tozer, B., Watts, A. B., & Daly, M. C., 2017. Crustal structure, gravity anomalies, and subsidence history of the Parnaíba cratonic basin, Northeast Brazil. *Journal of Geophysical Research: Solid Earth*, *122*, 5591–5621. https ://doi.org/10.1002/2017J B014348

Vogt, P.R., Anderson, C.J. & D.R. Bracey, D.R., 1973. Mesozoïc magnetic anomalies, sea floor spreading, and geomagnetic reversals in the southwestern North Atlantic, J. Geophys. Res., 76 20, 4796-4823.

Watts, A. B., Rodger, M., Peirce, C., Greenroyd, C.J. & Hobbs, R.W., 2009. Seismic structure, gravity anomalies, and flexure of the Amazon continental margin, NE Brazil. *Journal of Geophysical Research*, 114, B07103, doi:10.1029/2008JB006259.

Wessel, P., Smith, W.H.F., Scharroo, R. ; Luis, J. M. 2011. The Generic Mapping Tools (GMT) version 5, *Am. Geophys*. Union , Fall Meeting 2011, abstract id. IN21D-05.

White, R. S., McKenzie, D. and O'Nions, R., 1992. Oceanic crustal thickness from seismic measurements and rare earth element inversions. *J. Geophys. Res.*, **97**, 19,683-19,715.

Zelt C. A., 1999, Modelling strategies and model assessment for wide-angle seismic traveltime data, Geophysical Journal International, 183-204.

Zelt, C.A. & Ellis, R.M., 1988. Practical and efficient ray tracing in two-dimensional media for rapid traveltime and amplitude forward modelling. *Canadian Journal of Exploration Geophysics*, **24**, 16–31.

Zelt, C.A., Smith, R.B., 1992. Seismic travel time inversion for 2-D crustal velocity structure, *Geophysical Journal International*, **108**, 16–34.

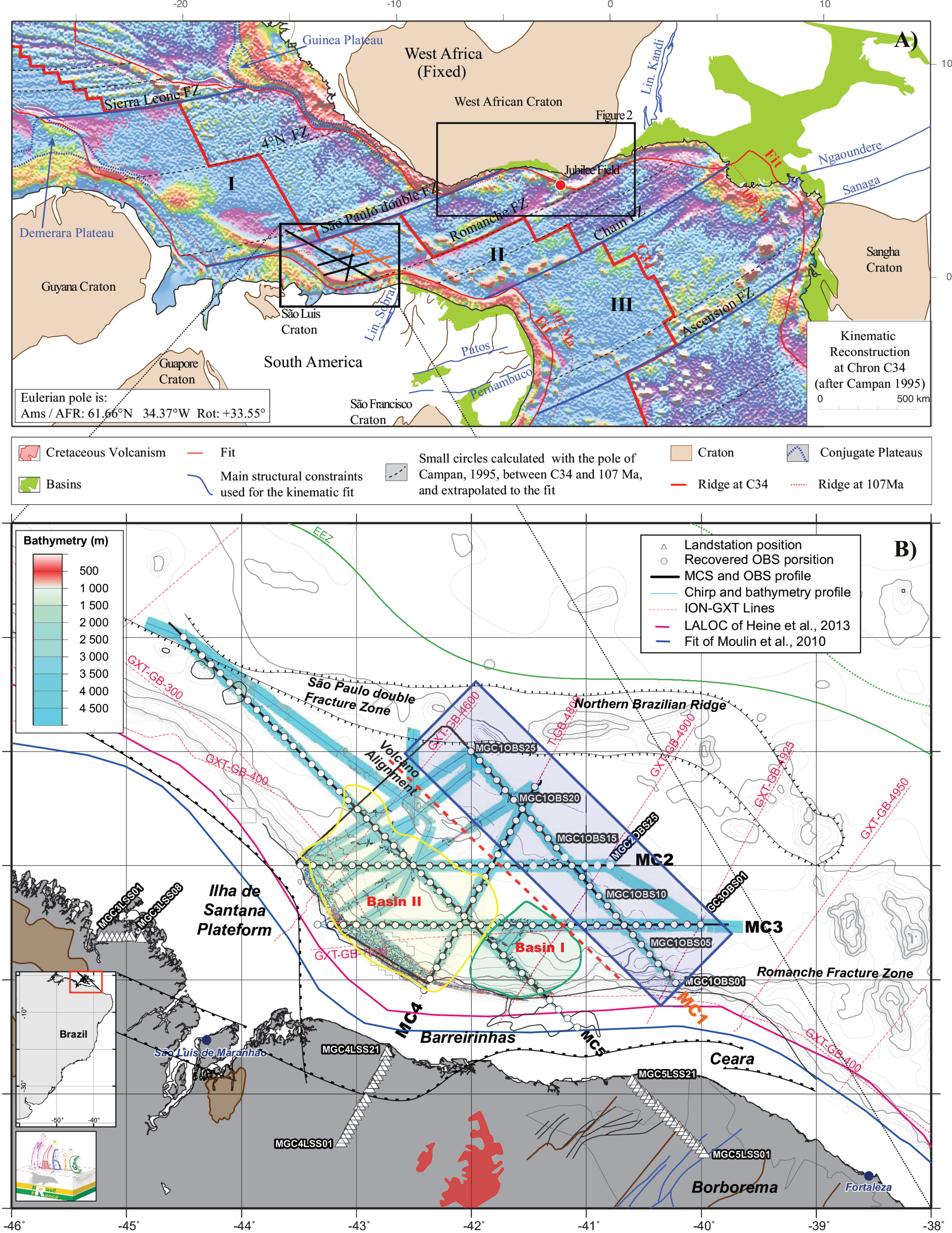

Figure 1 - Moulin et al.

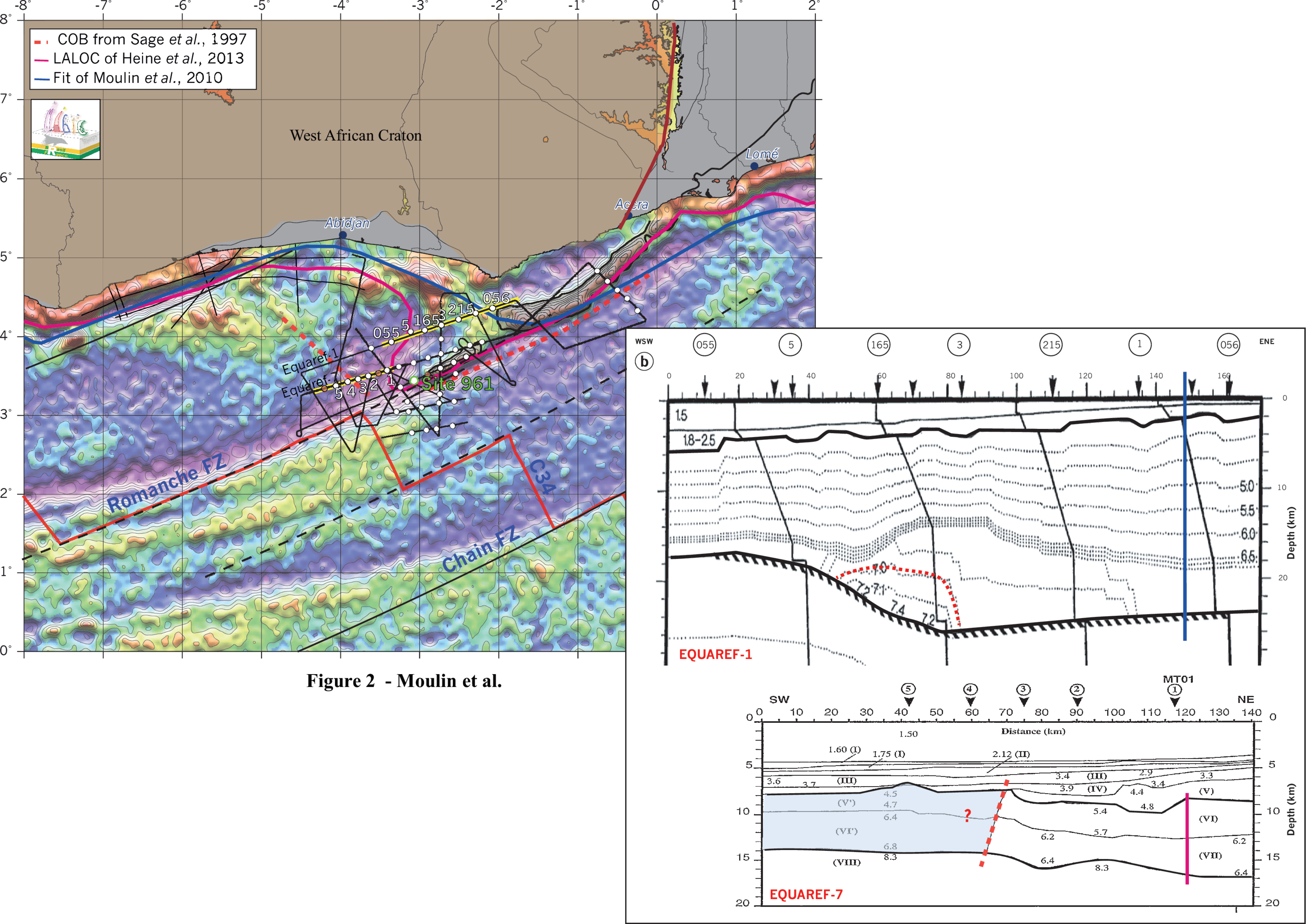

Figure 2 - Moulin et al.

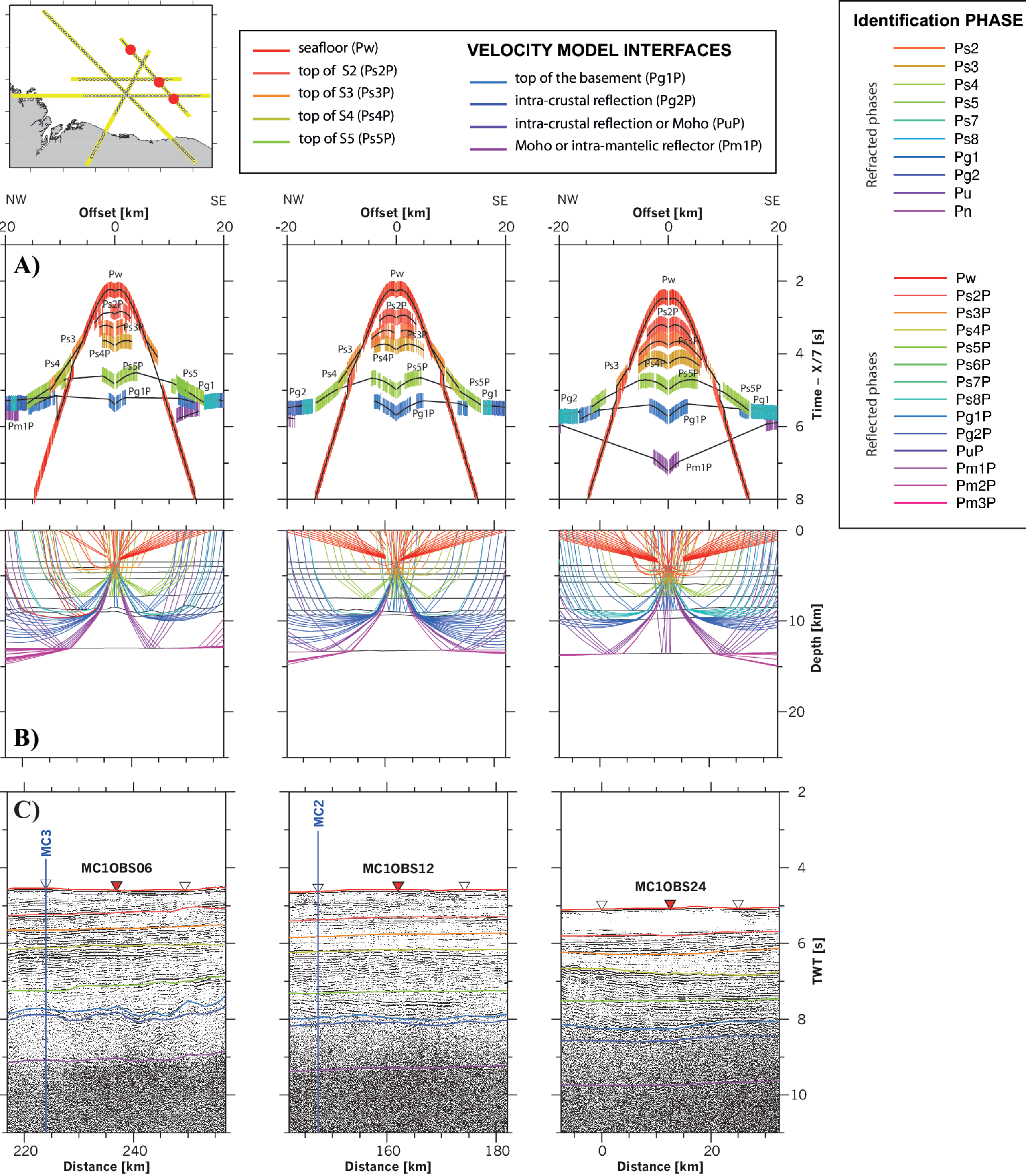

Figure 3 - Moulin et al.

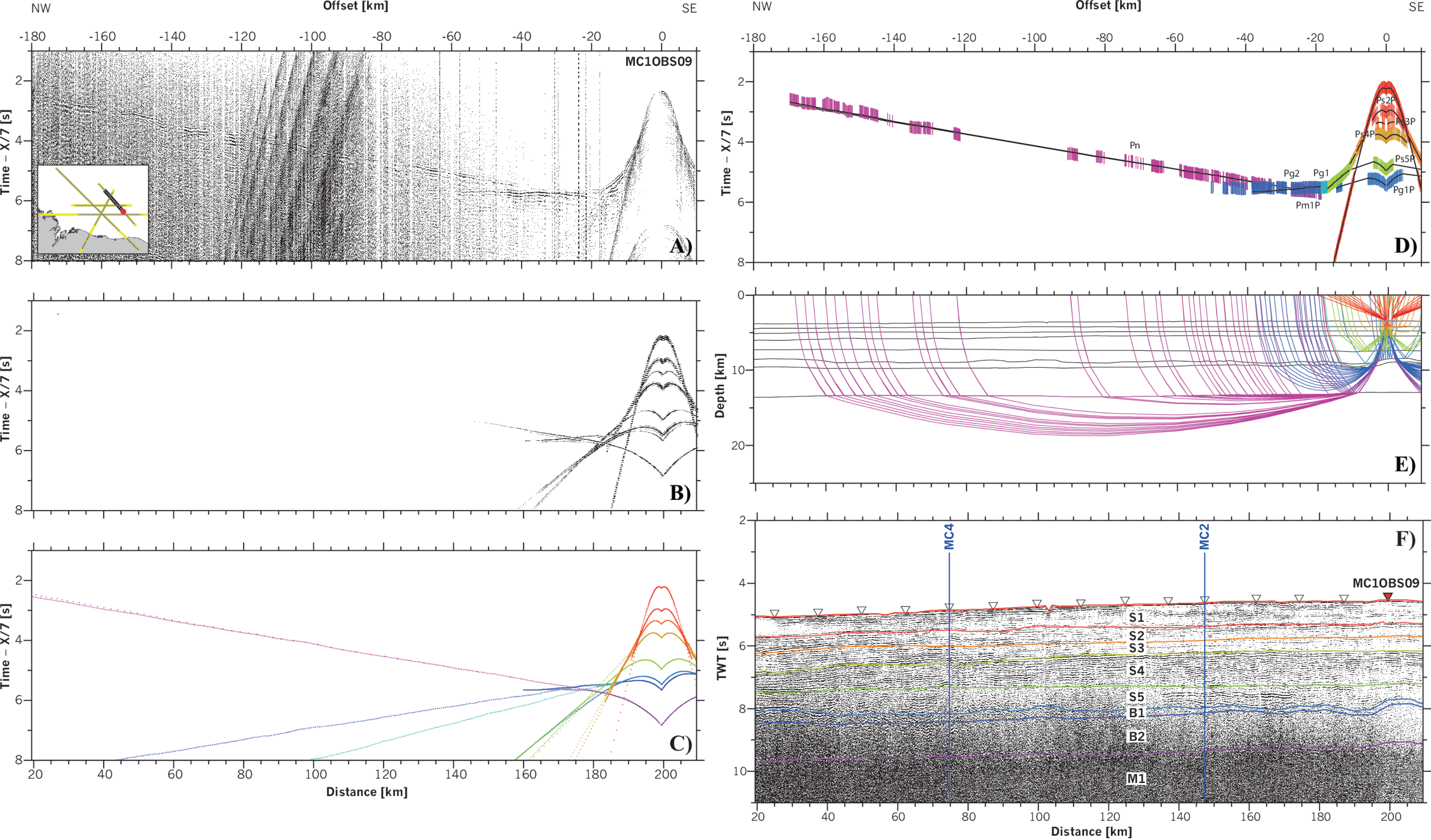

Figure 4 - Moulin et al.

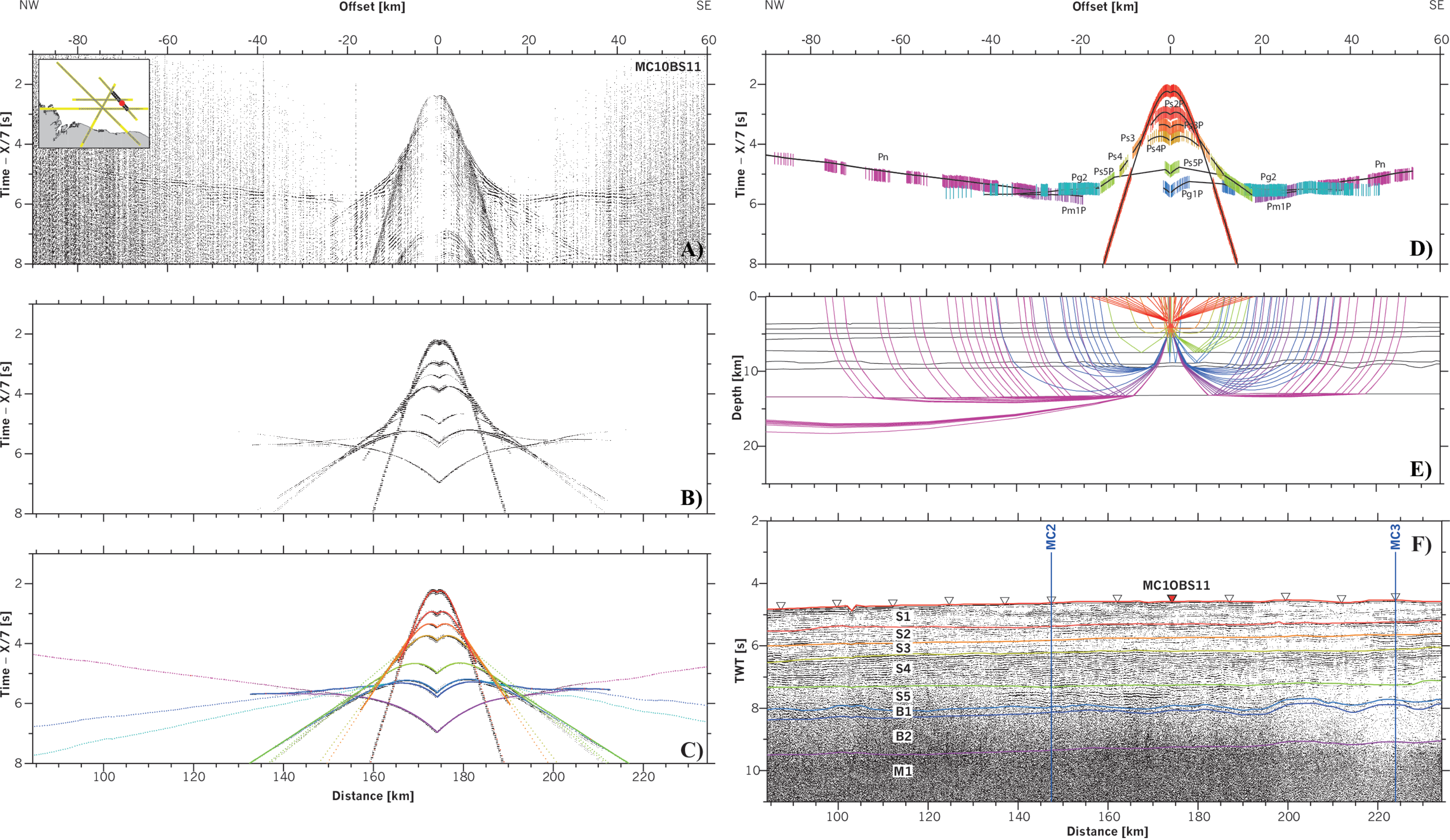

Figure 5 - Moulin et al.

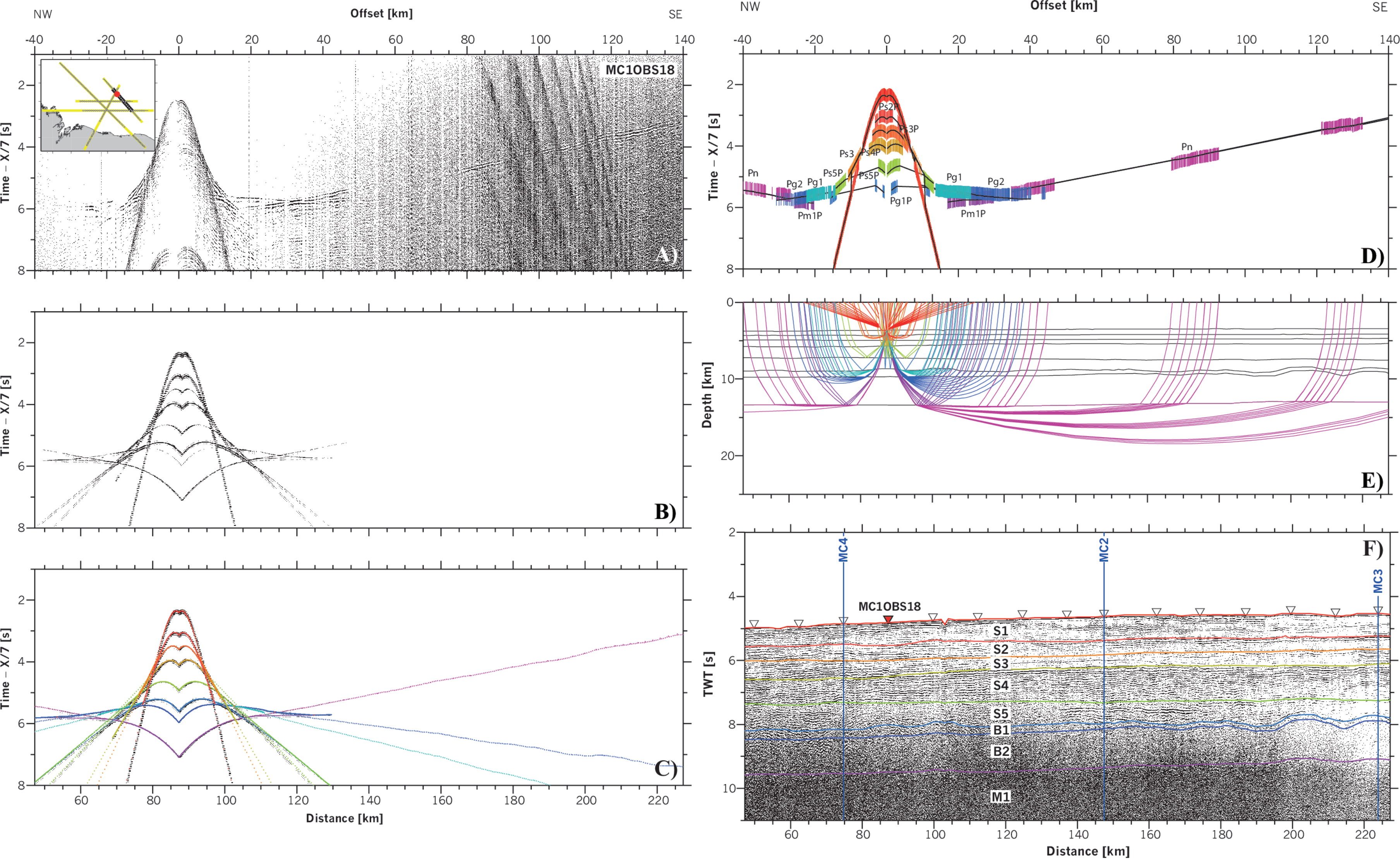

Figure 6 - Moulin et al.

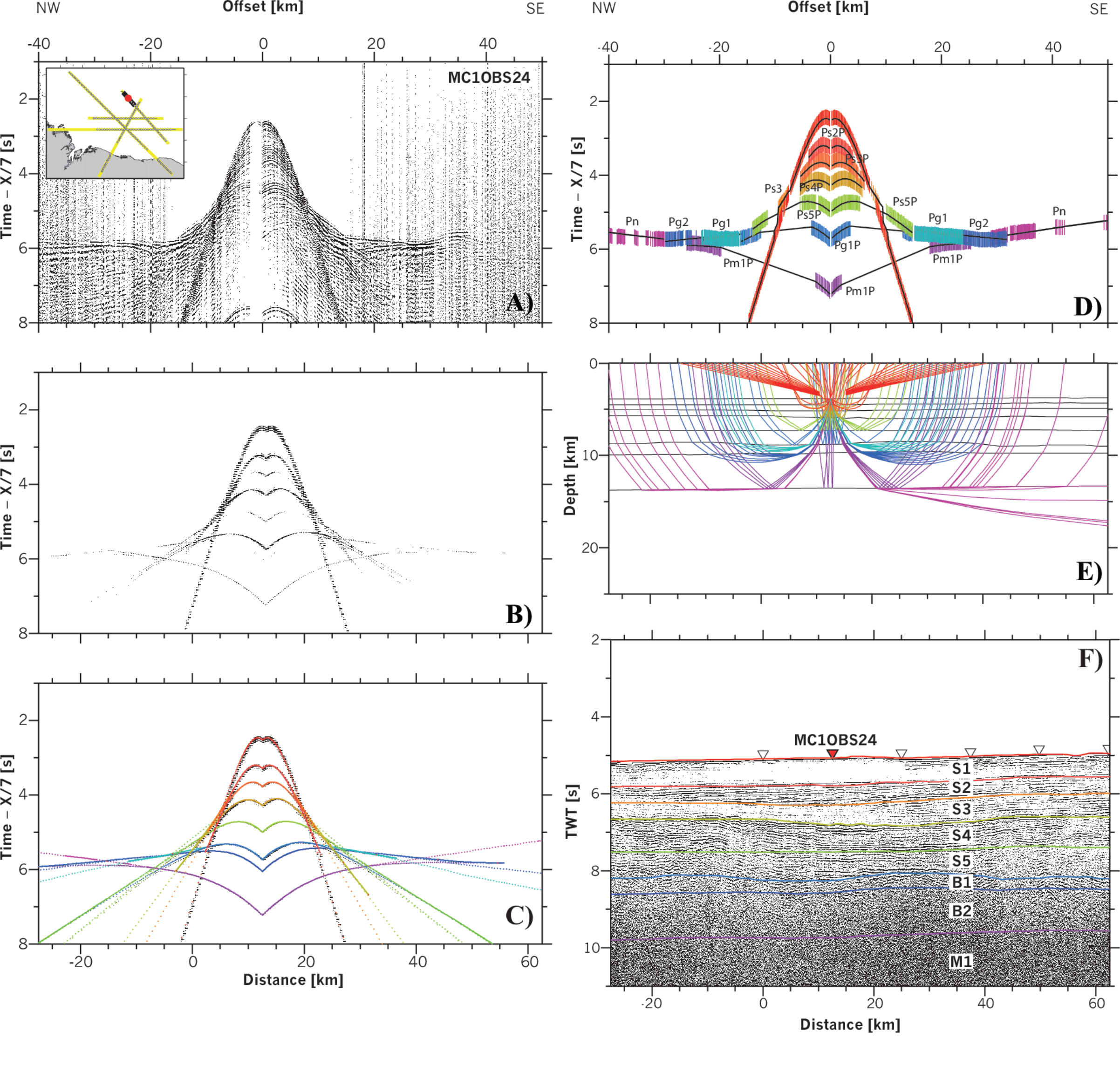

Figure 7 - Moulin et al.

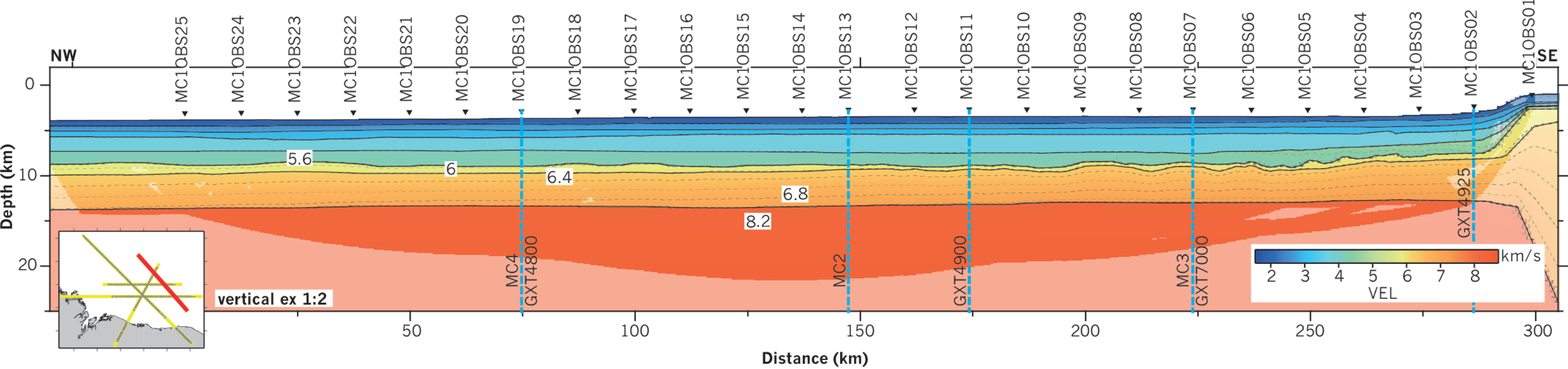

Figure 8 - Moulin et al.

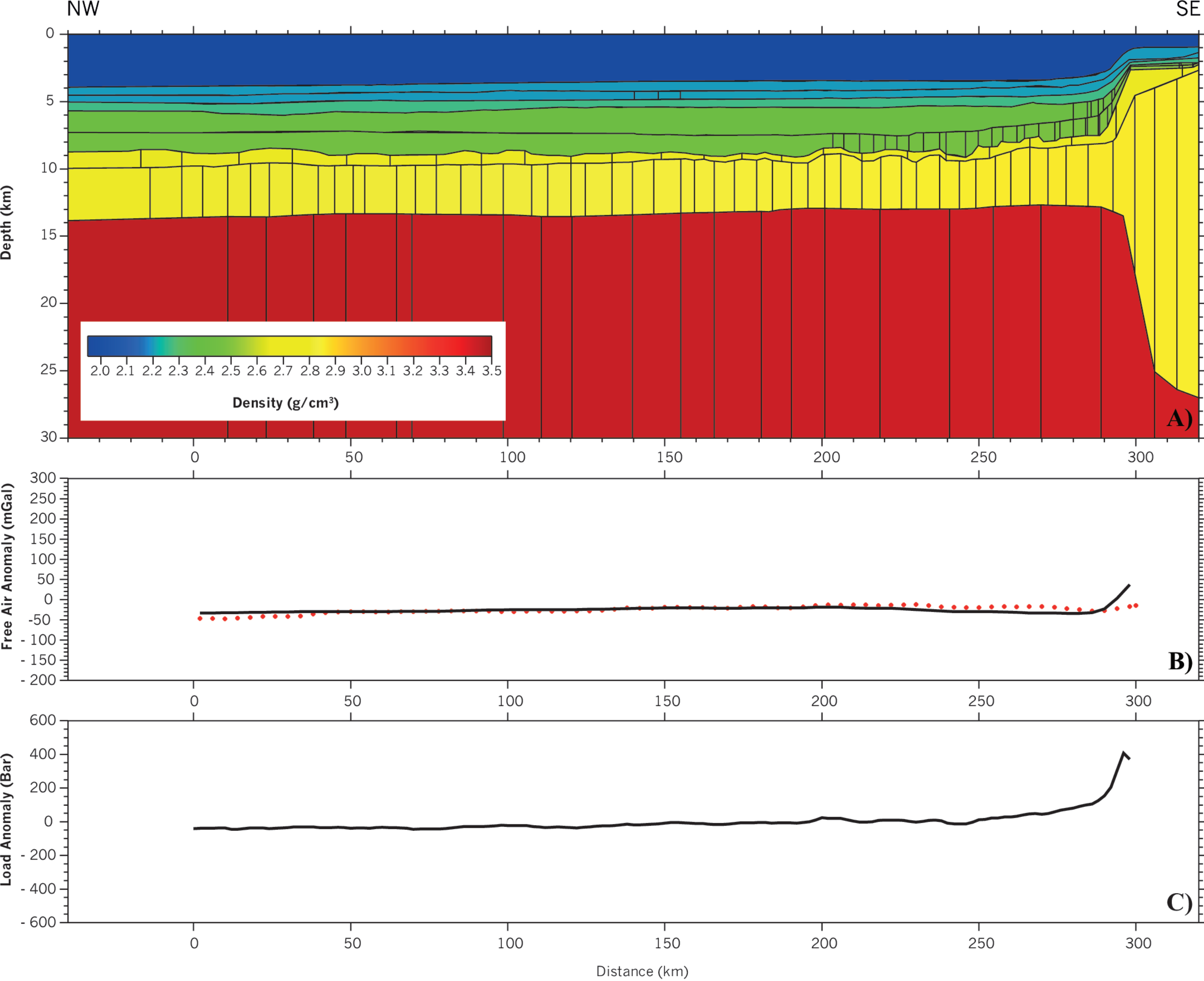

Figure 9 - Moulin et al.

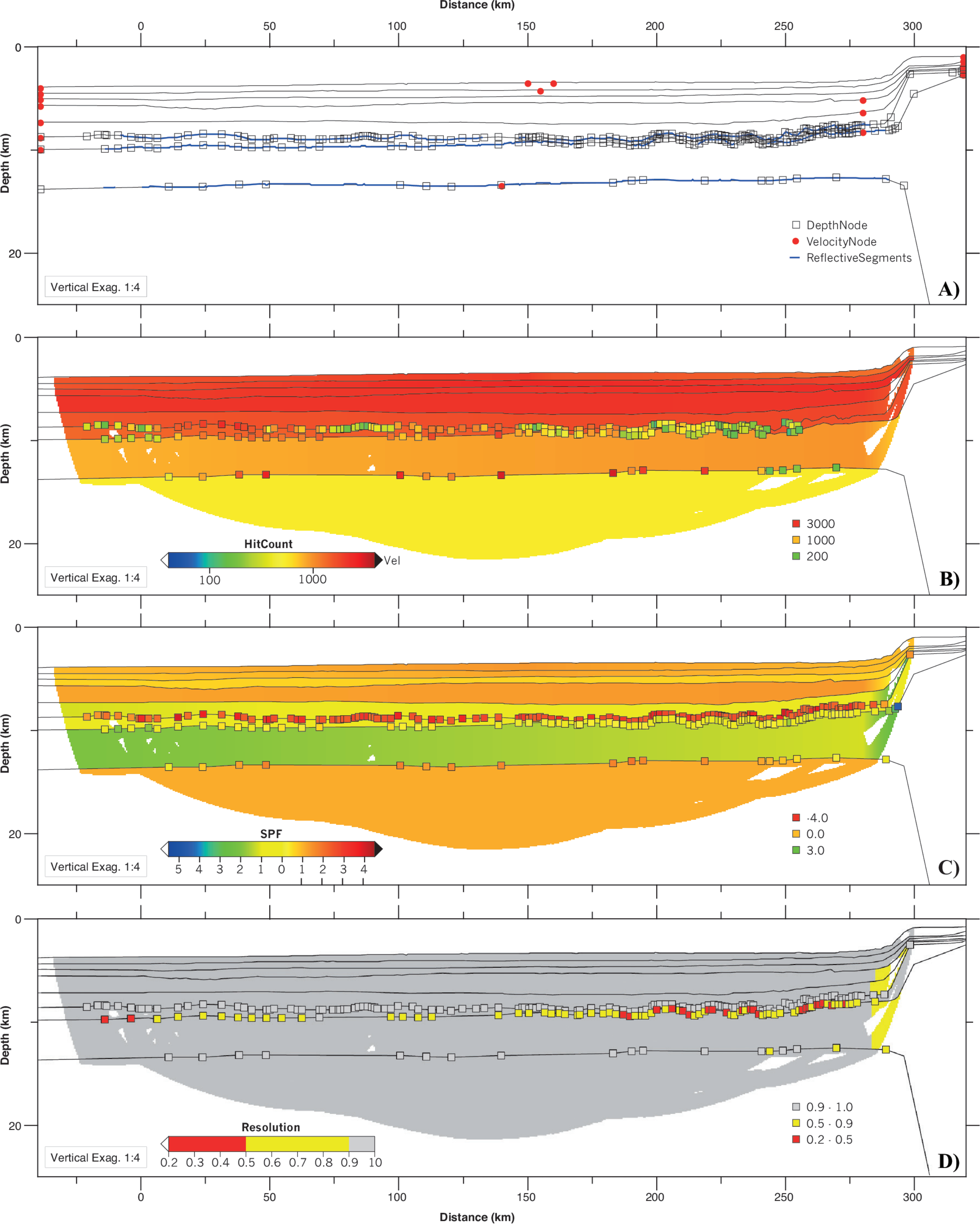

Figure 10 - Moulin et al.

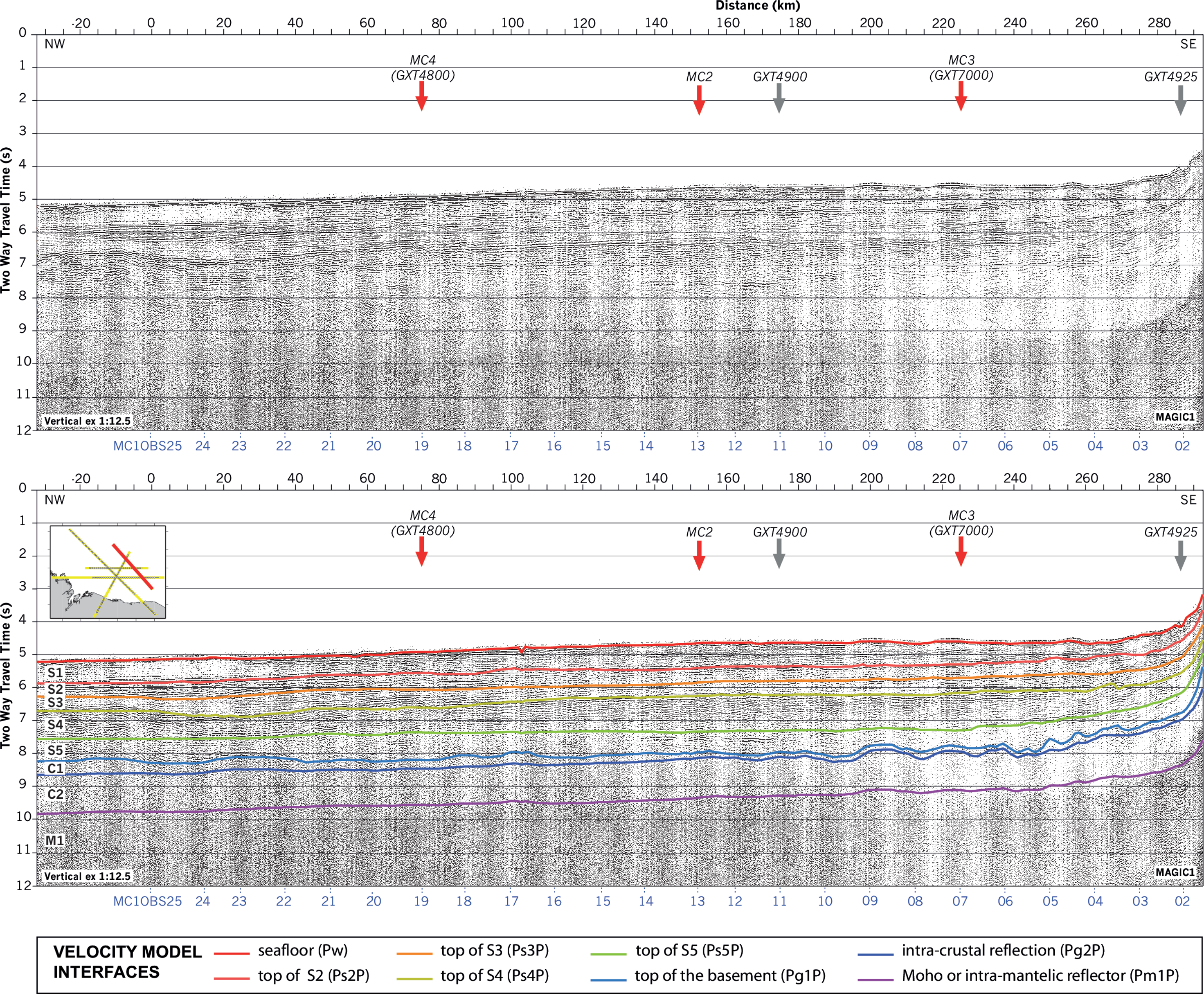

Figure 11 - Moulin et al.

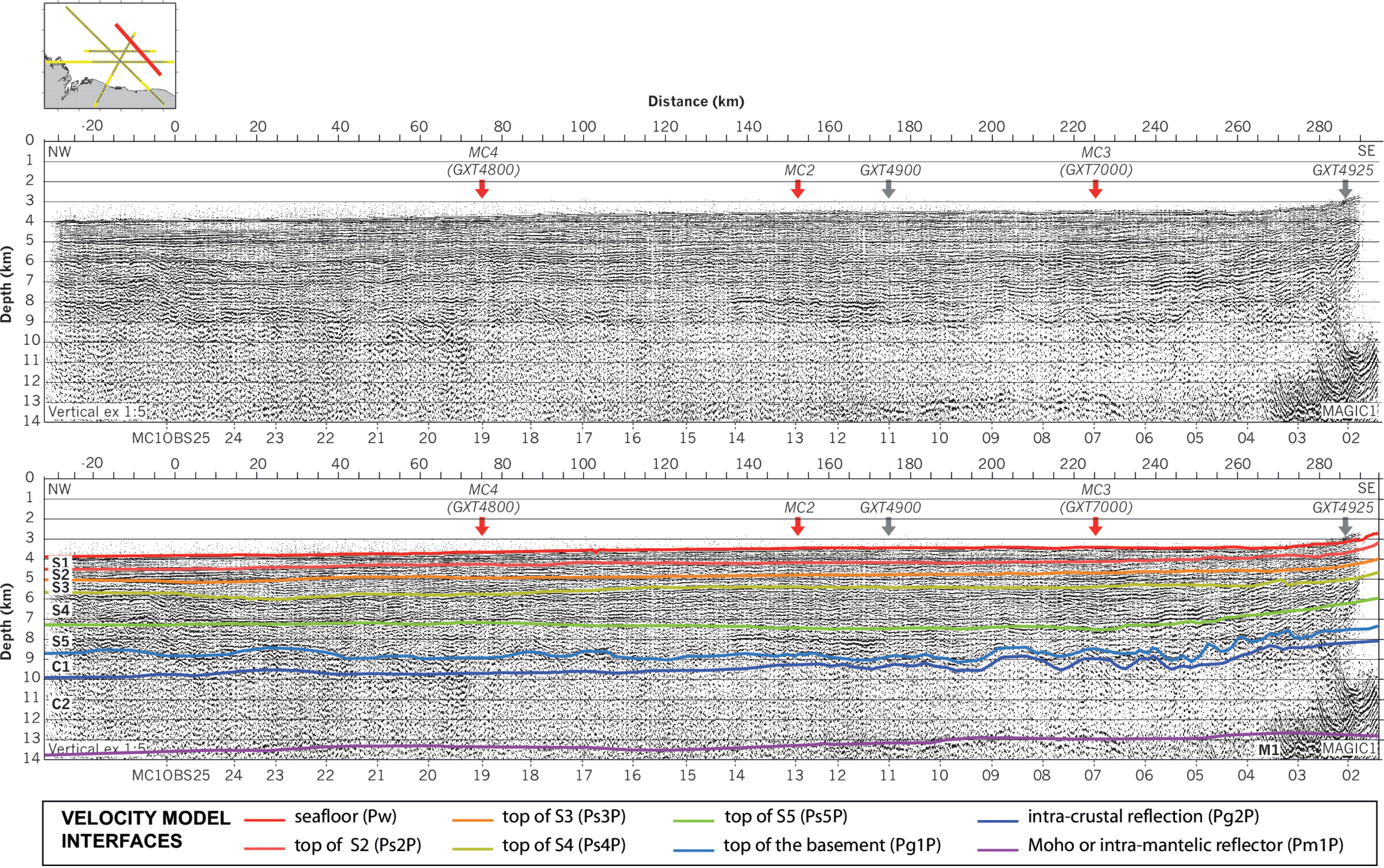

Figure 12 - Moulin et al.

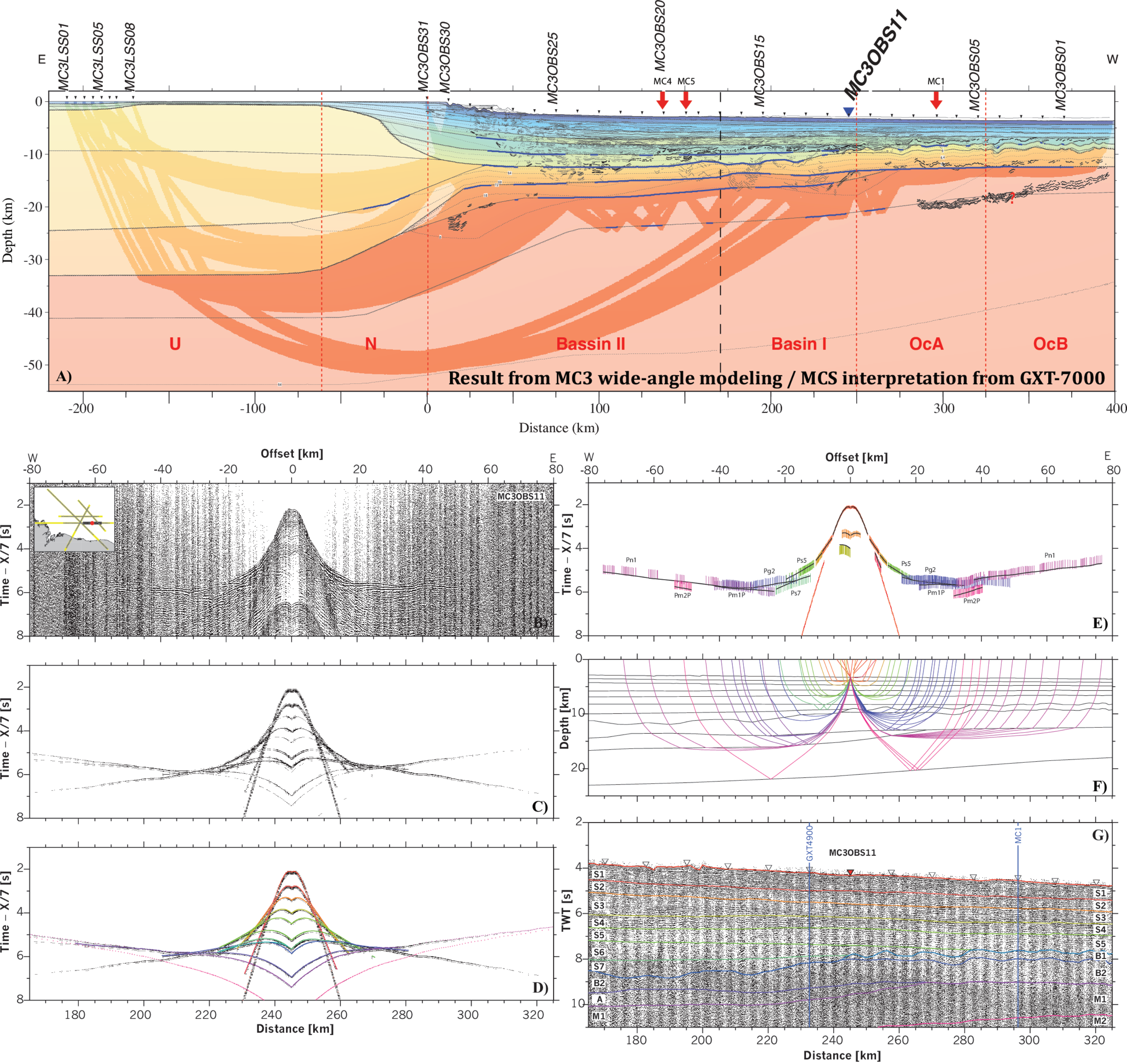

Figure 13 - Moulin et al.

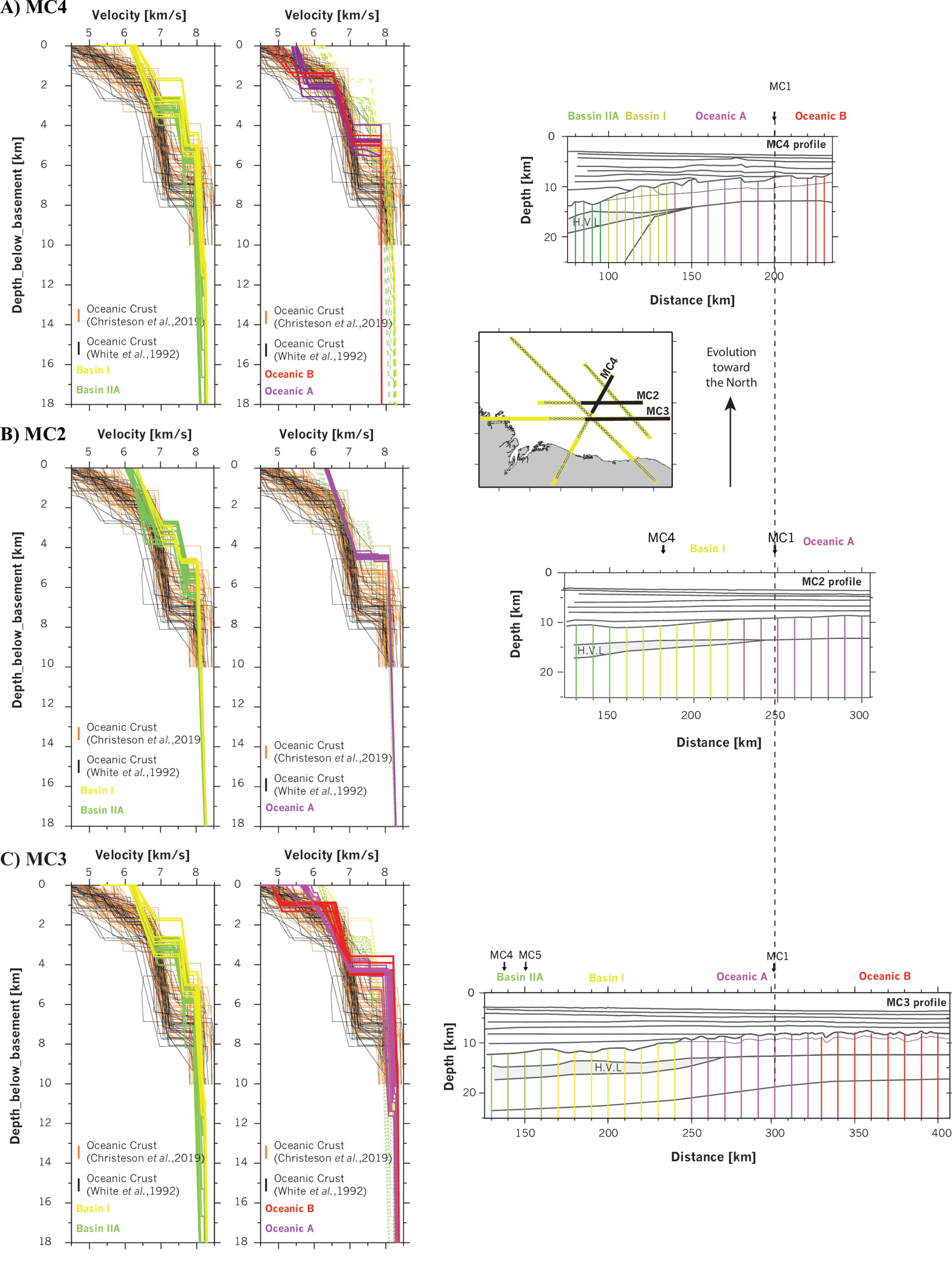

Figure 14 - Moulin et al.

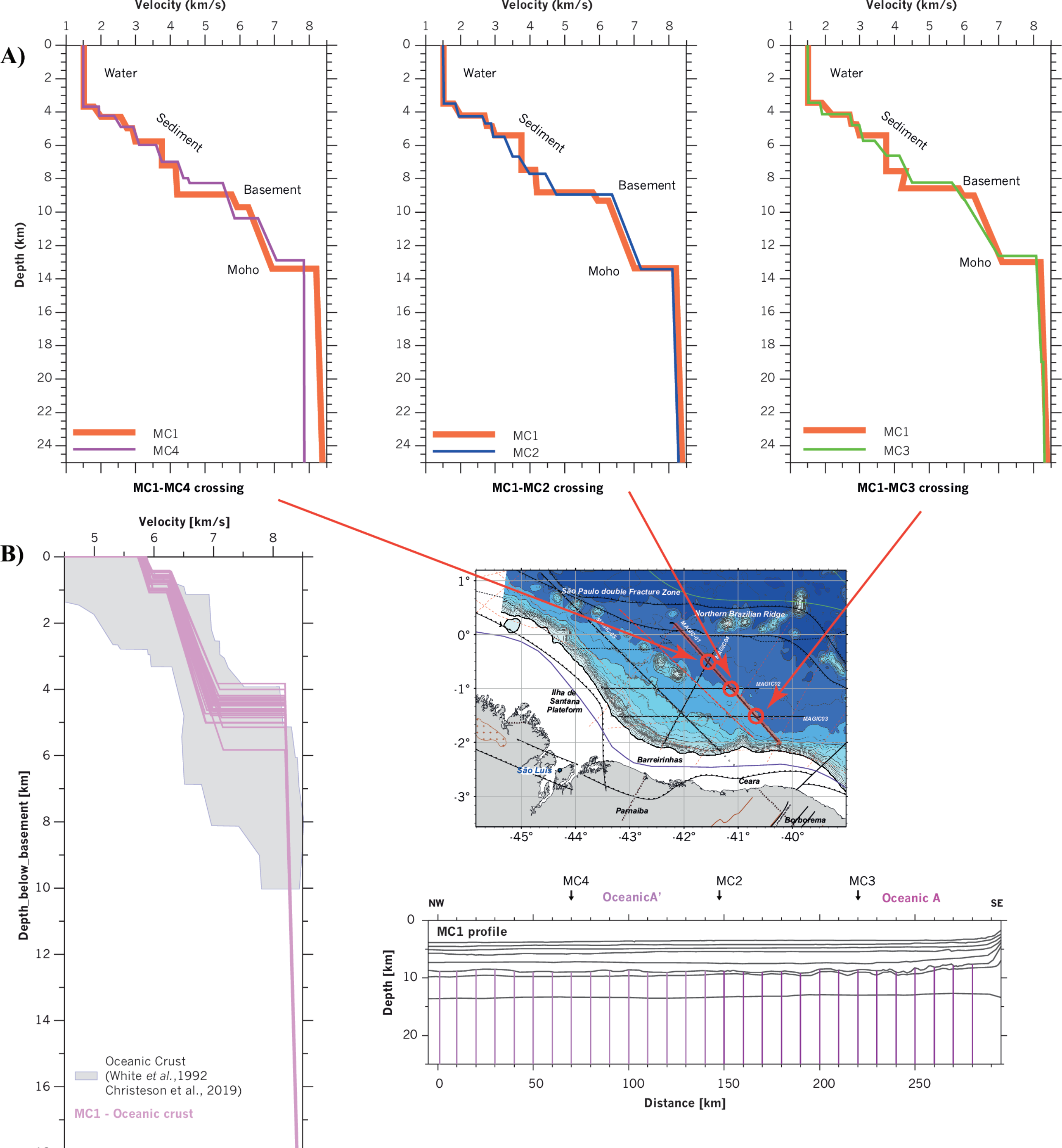

Figure 15 - Moulin et al.

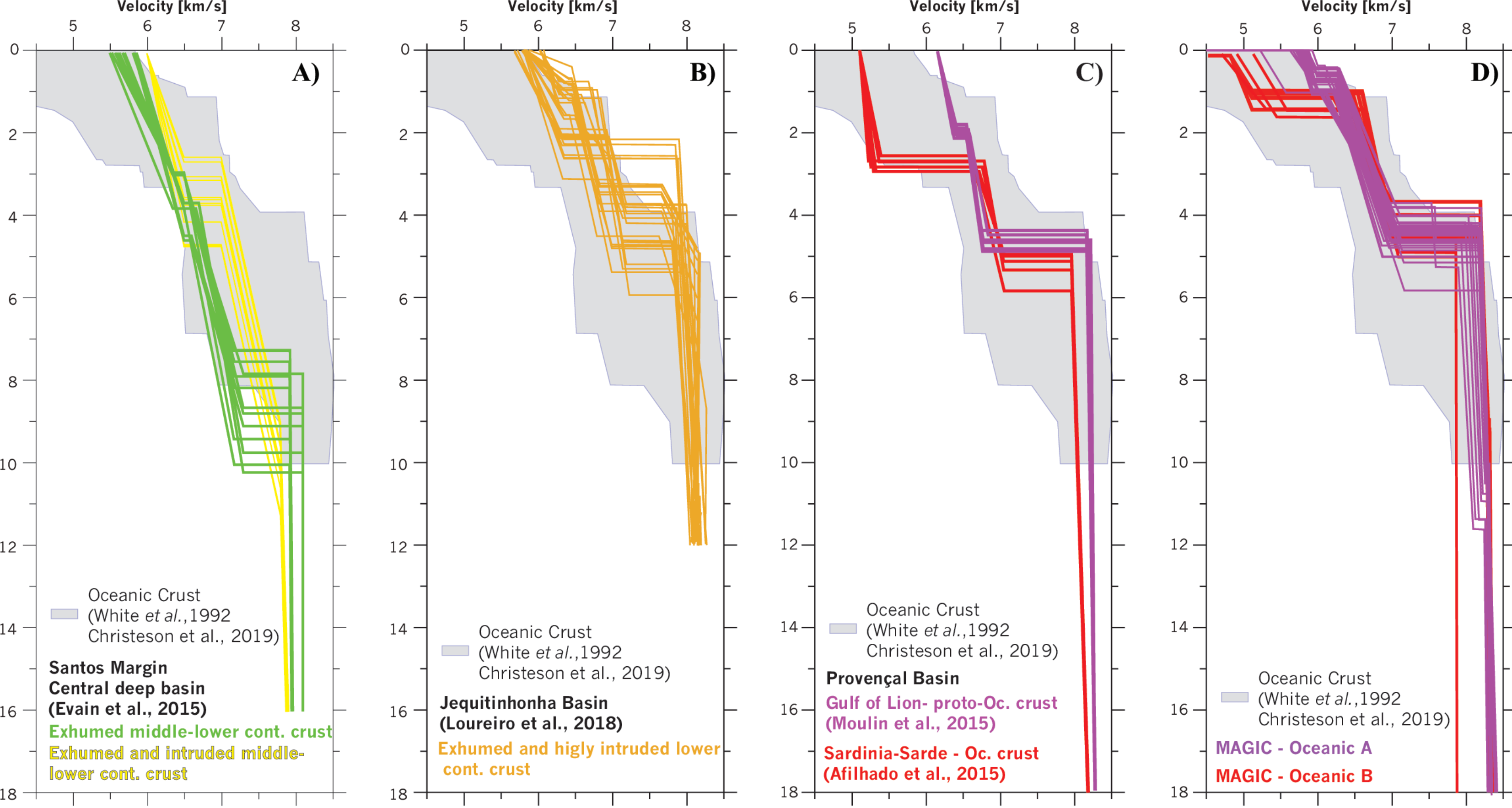

Figure 16 - Moulin et al.

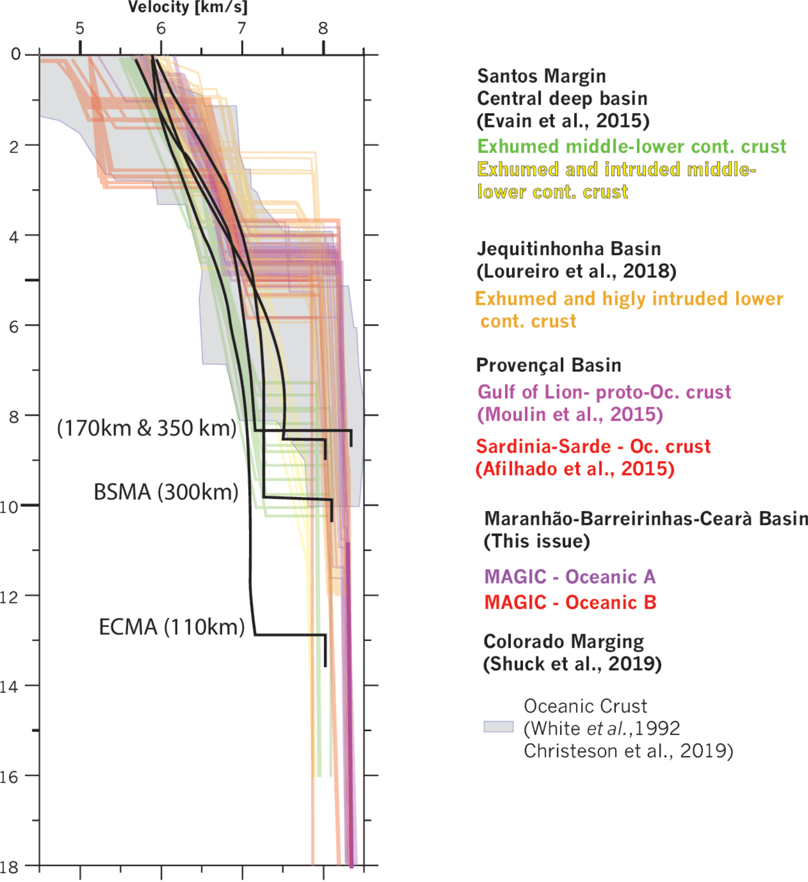

Figure 17 - Moulin et al.

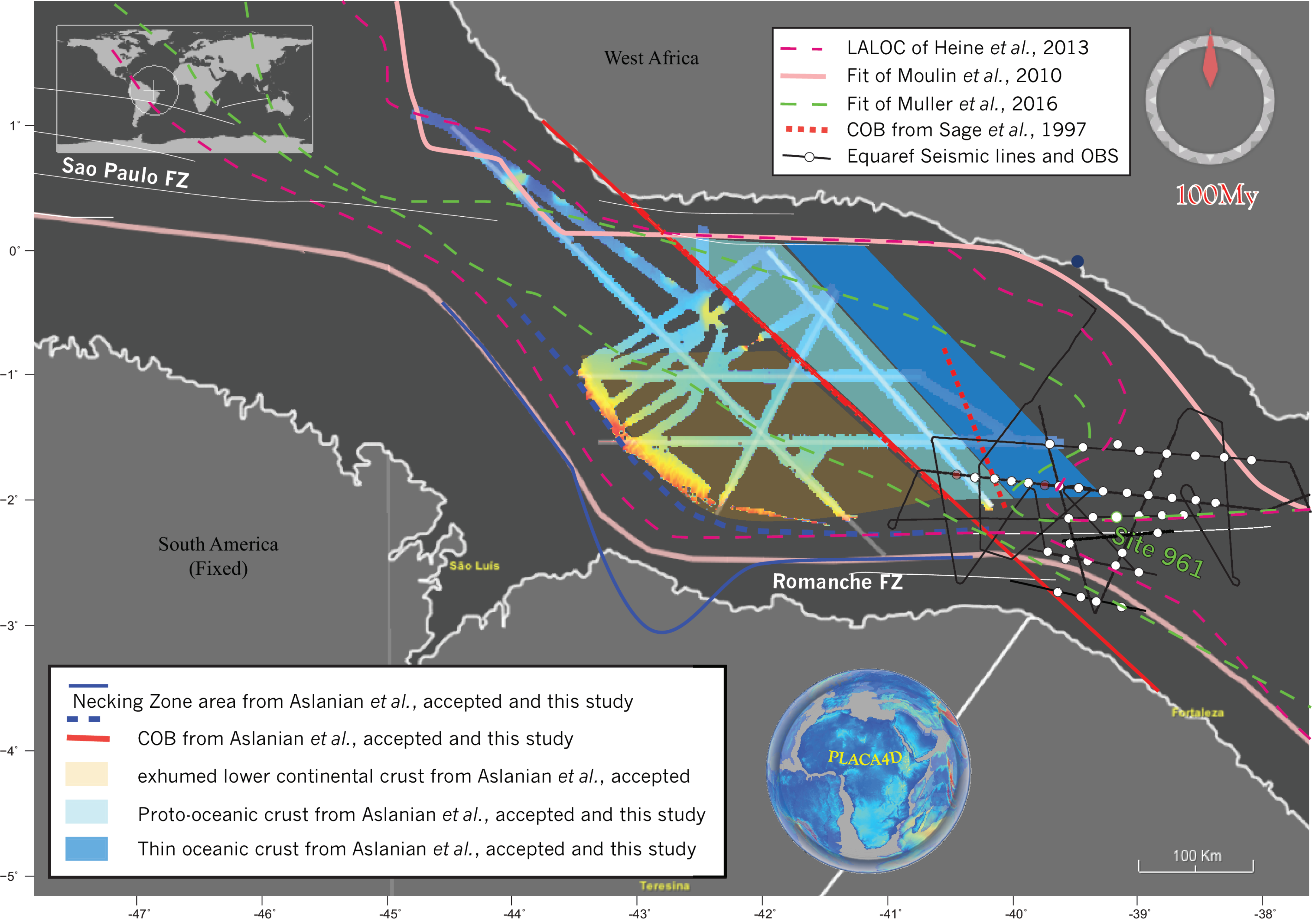

Figure 18 - Moulin et al.

MC01

Phase	npts	Trms	chi-squared
Pw	8883	0.017	0.028
Ps2P	1264	0.035	0.126
Ps3	707	0.066	0.434
Ps3P	1396	0.050	0.246
Ps4	652	0.093	0.875
Ps4P	1458	0.036	0.132
Ps5P	2721	0.074	0.542
Pg1/Pg2	6392	0.076	0.583
Pg1P	1953	0.058	0.333
Pm1P	3032	0.051	0.262
Pn	6198	0.079	0.627
All phases	34656	0.060	0.356

Table 1: Reflected or refracted phase name, number of explained events, residual mean-square, and normalized chi-squared value for all phases and the complete model of profile MC1 profile.

Instrument	shot	dir	npts	Trms	Chi-squared
MC1OBS01	299.213	-1	717	0.066	0.434
MC1OBS02	286.339	1	143	0.048	0.234
	286.339	-1	580	0.052	0.269
MC1OBS03	274.119	1	740	0.053	0.279
	274.119	-1	491	0.092	0.848
MC1OBS04	261.817	1	650	0.062	0.390
	261.817	-1	633	0.056	0.313
MC1OBS05	249.396	1	805	0.068	0.467
	249.396	-1	762	0.048	0.232
MC1OBS06	236.906	1	923	0.055	0.306
	236.906	-1	598	0.050	0.254
MC1OBS07	223.935	1	793	0.044	0.192
	223.935	-1	750	0.057	0.325
MC1OBS08	211.952	1	939	0.055	0.308
	211.952	-1	718	0.035	0.125
MC1OBS09	199.476	1	966	0.055	0.297
	199.476	-1	670	0.033	0.112
MC1OBS10	186.967	1	1169	0.057	0.327
	186.967	-1	694	0.036	0.132
MC1OBS11	174.216	1	715	0.062	0.387
	174.216	-1	666	0.057	0.326
MC1OBS12	162.041	1	696	0.075	0.570
	162.041	-1	705	0.046	0.213
MC1OBS13	147.385	1	693	0.077	0.590
	147.385	-1	832	0.048	0.233
MC1OBS14	137.046	1	534	0.046	0.215
	137.046	-1	679	0.056	0.314
MC1OBS15	124.667	1	573	0.050	0.250
	124.667	-1	851	0.069	0.470
MC1OBS16	112.174	1	680	0.060	0.360
	112.174	-1	966	0.090	0.810
MC1OBS17	99.701	1	518	0.068	0.463
	99.701	-1	829	0.061	0.368
MC1OBS18	87.222	1	559	0.042	0.178
	87.222	-1	897	0.057	0.321
MC1OBS19	74.701	1	496	0.049	0.243
	74.701	-1	552	0.071	0.502
MC1OBS20	62.283	1	670	0.062	0.386
	62.283	-1	530	0.061	0.369
MC1OBS21	49.807	1	619	0.061	0.370
	49.807	-1	755	0.064	0.415
MC1OBS22	37.415	1	688	0.056	0.312
	37.415	-1	1084	0.095	0.911
MC1OBS23	24.958	1	493	0.052	0.273
	24.958	-1	773	0.068	0.467
MC1OBS24	12.542	1	727	0.044	0.194
	12.542	-1	818	0.047	0.221
MC1OBS25	0.000	1	630	0.050	0.247
	0.000	-1	687	0.045	0.204

Table 2: Instrument name, distance along model, direction code, number of explained events, residual mean-square, and normalized chi-squared value for each OBS of the MC1 profile.